Journal of Medicinal Chemistry

pubs.acs.org/jmc

Article

Synthetic Approaches to Novel Human Carbonic Anhydrase Isoform Inhibitors Based on Pyrrol-2-one Moiety

Cristina M. Al-Matarneh,* Mariana Pinteala,* Alina Nicolescu, Mihaela Silion, Francesca Mocci, Razvan Puf, Andrea Angeli,* Marta Ferraroni, Claudiu T. Supuran, Susi Zara, Simone Carradori, Niccolò Paoletti, Alessandro Bonardi, and Paola Gratteri

Cite This: *J. Med. Chem.* 2024, 67, 3018−3038

Read Online

ACCESS | Metrics & More | Article Recommendations | Supporting Information

ABSTRACT: New dihydro-pyrrol-2-one compounds, featuring dual sulfonamide groups, were synthesized through a one-pot, three-component approach utilizing trifluoroacetic acid as a catalyst. Computational analysis using density functional theory (DFT) and condensed Fukui function explored the structure−reactivity relationship. Evaluation against human carbonic anhydrase isoforms (hCA I, II, IX, XII) revealed potent inhibition. The widely expressed cytosolic hCA I was inhibited across a range of concentrations (K_I 3.9−870.9 nM). hCA II, also cytosolic, exhibited good inhibition as well. Notably, all compounds effectively inhibited tumor-associated hCA IX (K_I 1.9−211.2 nM) and hCA XII (low nanomolar). Biological assessments on MCF7 cancer cells highlighted the compounds' ability, in conjunction with doxorubicin, to significantly impact tumor cell viability. These findings underscore the potential therapeutic relevance of the synthesized compounds in cancer treatment.

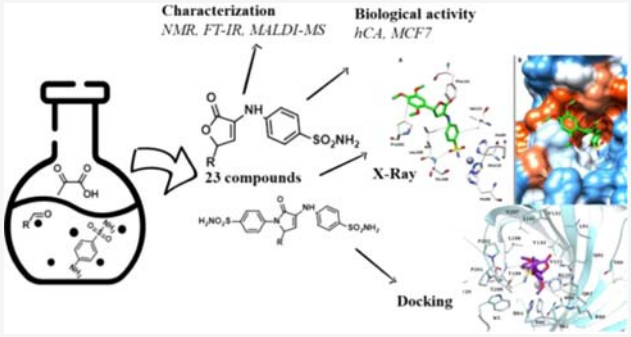

INTRODUCTION

2,5(H)-Pyrrol-2-one (DPO), a key component of numerous bioactive compounds or precursors, is found in large quantities in pheromones, alkaloids, steroids, heme, chlorophylls, and other substances. There are numerous pyrrol-2-one-modified bioactive natural compounds, including pyrrocidine A, quinolactacin C, ypaoamide, holomycin, and thiolutin.[1] DPO possesses a broad range of activities such as very potent antibacterial activity,[2−5] FPR1 antagonism,[6] cytotoxic and antitumor properties,[7,8] tyrosinase inhibition,[9] antioxidant activity,[8] carbonic anhydrase inhibition,[10] or modulation of the annexin A2−S100A10 protein interaction.[11] The synthesis of DPO derivatives can be done in a variety of ways nowadays, including the multistep method,[12−15] the two-component approach,[16−19] the three-component method,[20,21] the multicomponent method, and others.[22] That is why there is still a need to develop a milder and more effective one-pot synthesis approach for these significant heterocycles. An innovative tandem reaction involving two simple components—amines and aldehydes—was an approach to generate DPO derivatives.[23]

A widespread family of metalloenzymes called carbonic anhydrases (CAs) catalyzes the reversible transformation of carbon dioxide to H^+ and HCO^{3-}.[24,25]

Many biosynthetic processes, like respiration, photosynthesis, pH regulation, and electrolyte secretion, are carried out by CA enzymes.[26,27] In humans, there are currently 15 known isoforms, of which only 12 are catalytically active. Five of them are cytosolic (hCA I, II, III, VII, and XIII), two are mitochondrial (hCA VA and VB), one secretory (hCA VI), and the rest membrane-bound (hCA IV, IX, XII, and XIV).

Sulfonamide derivatives, which coordinate the zinc ion with their terminal deprotonated nitrogen atom, are the traditional CA inhibitors (CAIs), which have been used in therapeutic settings for more than 70 years as diuretics and antiglaucoma medications[28] due to their chemical stability and straightforward production.

Recently, hCA IX has often been considered a surrogate marker of tumor hypoxia and is widely regarded as an important biomarker of poor prognosis for many solid tumors.[29]

Aiming to produce new derivatives in light of all of the above, our current work was a continuation of our earlier investigation into *N*-heterocycle systems[30−32] and as part of our interest in the field of physiologically active chemicals,[33−39]

Received: November 22, 2023
Revised: January 10, 2024
Accepted: January 11, 2024
Published: February 1, 2024

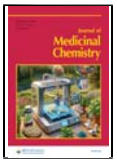

https://doi.org/10.1021/acs.jmedchem.3c02190
J. Med. Chem. 2024, 67, 3018−3038

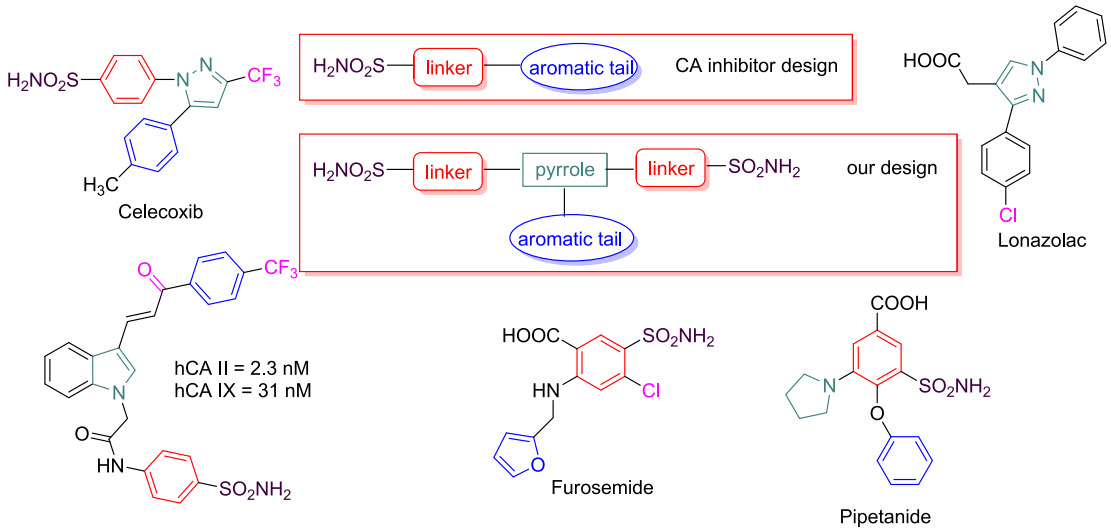

Figure 1. Design in the series of the target pyrrole-based bis-sulfonamide derivatives.

Scheme 1. Reaction Pathway to Compounds 1−23

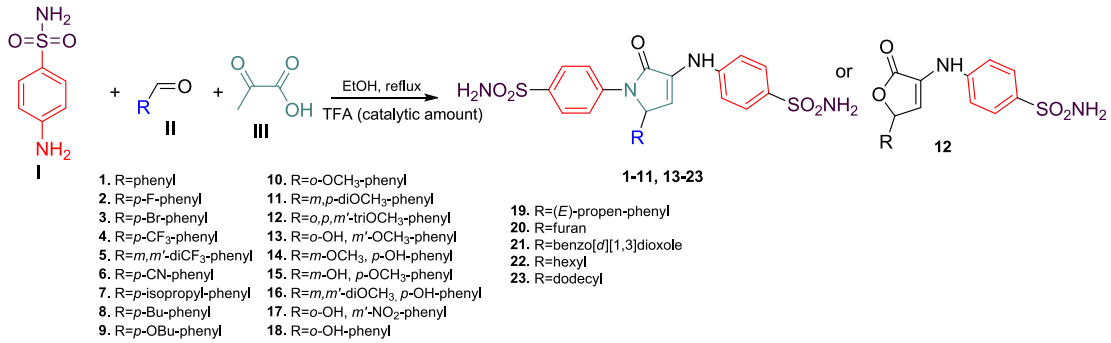

1. R=phenyl
2. R=*p*-F-phenyl
3. R=*p*-Br-phenyl
4. R=*p*-CF_3-phenyl
5. R=*m,m'*-diCF_3-phenyl
6. R=*p*-CN-phenyl
7. R=*p*-isopropyl-phenyl
8. R=*p*-Bu-phenyl
9. R=*p*-OBu-phenyl
10. R=*o*-OCH_3-phenyl
11. R=*m,p*-diOCH_3-phenyl
12. R=*o,p,m'*-triOCH_3-phenyl
13. R=*o*-OH, *m'*-OCH_3-phenyl
14. R=*m*-OCH_3, *p*-OH-phenyl
15. R=*m*-OH, *p*-OCH_3-phenyl
16. R=*m,m'*-diOCH_3, *p*-OH-phenyl
17. R=*o*-OH, *m'*-NO_2-phenyl
18. R=*o*-OH-phenyl
19. R=(*E*)-propen-phenyl
20. R=furan
21. R=benzo[*d*][1,3]dioxole
22. R=hexyl
23. R=dodecyl

with a focus on carbonic anhydrase inhibitors.[24,26,28,40−45] The synthesis, structure, and evaluation of several novel dihydropyrrol-2-one derivatives as inhibitors of tumor-associated human CA are thus reported here.

RESULTS AND DISCUSSIONS

Synthesis and Characterization. Investigated structures that have effective binding capabilities in the CA site mainly contain the sulfonamide pharmacophore moiety.[28] Our aim was to synthesize hybrid molecules characterized by pyrrol-2-one as a core and two active binding groups on its sides (Figure 1). In order to obtain the proposed derivatives, *para*-amino sulfonamide (**I**) was reacted with aldehyde derivatives possessing aromatic, aliphatic, or cyclic structures (**II**) and pyruvic acid (**III**) in ethanol in the presence of catalytic amounts of trifluoroacetic acid (Scheme 1).

The library of newly synthesized compounds consists of 1*H*-pyrrol-2(5*H*)-one derivatives **1**−**11** and **13**−**23** as a common pattern along with the 2-oxo-2,5-dihydrofuran derivative, compound **12**. Among the synthesized compounds, we have integrated different substituents on the phenyl ring that vary by electron-donating to electron-withdrawing effects, from one to three substituents and different substitution positions, oxygen-containing heterocycles (furan and piperonal), or aliphatic substituents as reported in Figure 2.

All of the compounds were obtained in good yields (between 47 and 88%) and bidimensional correlation experiments provided the clear proton and carbon signal assignments for all novel compounds that are detailed in the Experimental Section. As support of the Experimental Section, in the Supporting Information (SI) are presented ^{1}H, ^{13}C, ^{19}F, ^{1}H,^{13}C HMBC, ^{1}H,^{15}N-HMBC, IR, and matrix-assisted laser desorption ionization-mass spectrometry (MALDI-MS) spectra of some representative novel compounds.

For the majority of investigated benzenesulfonamide derivatives, most of the proton and carbon atoms have resonance signals in the low-field regions: above 6 ppm in ^{1}H NMR and 100 ppm in ^{13}C NMR spectra. Proton and proton−carbon spin systems information was obtained from homo- and heteronuclear bidimensional correlation experiments like H,H-COSY, H,C-HSQC, and H,C-HMBC. Four doublets in the range of 7.40−7.90 ppm in the ^{1}H NMR spectra (as an example ^{1}H NMR spectrum of compound **1** in Figure S1 and Experimental Section), exhibiting the roof-effect characteristic of para-substitution, were easily attributed to the two nonequivalent *para*-benzenesulfonamide rings. Throughout this series, their presence in ^{1}H NMR spectra was a fast indicator for the formation of derivatives with the pyrrol-2(5*H*)-one cycle. For almost all investigated compounds, the two protons from the pyrrol-2(5*H*)-one cycle appear in the interval 6.20−6.80 ppm as doublets with a 2 or 3 Hz vicinal coupling constant (Figures S1−S6 and Experimental Section). In the case of **22** and **23** compounds, when aliphatic aldehydes were used as starting materials, pyrrole H-5 signal shifted 1

https://doi.org/10.1021/acs.jmedchem.3c02190
J. Med. Chem. 2024, 67, 3018−3038

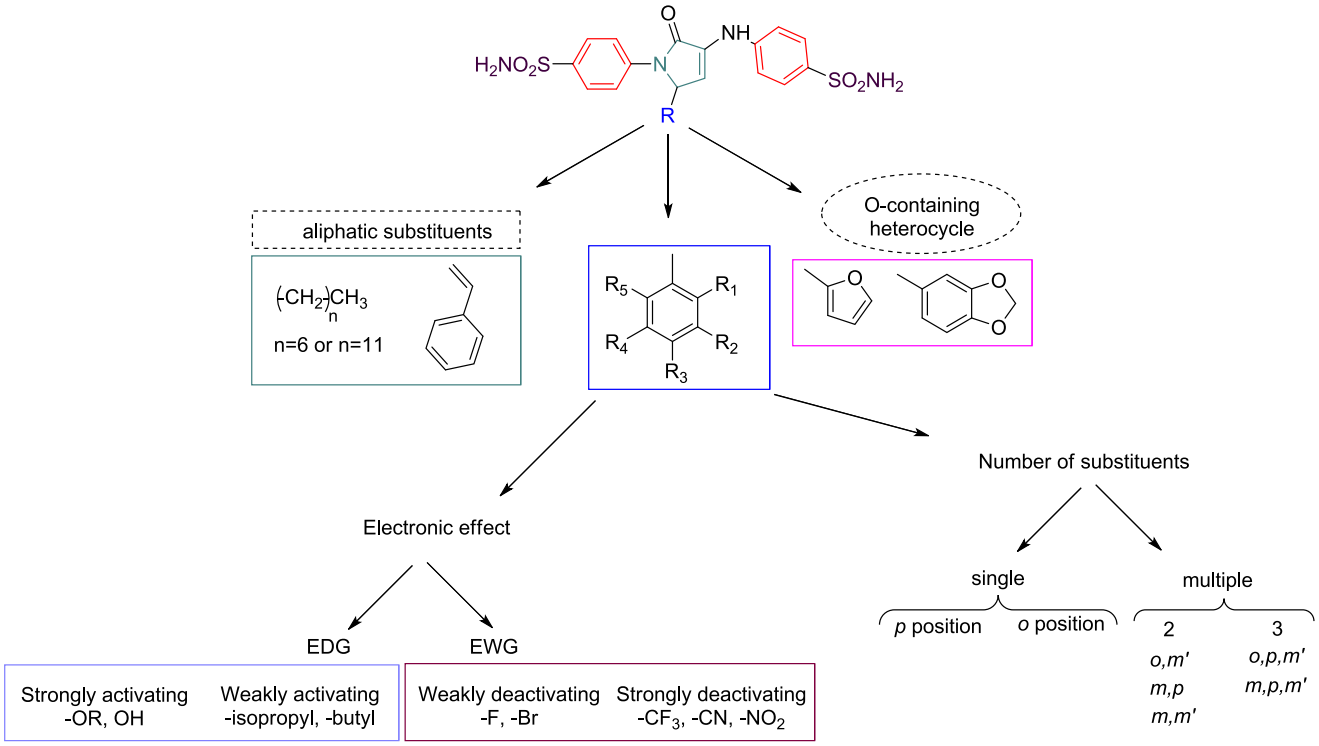

Figure 2. Rational choice of the substituents.

ppm upfield and appeared as a multiplet due to vicinal couplings with both pyrrole H-4 and methylene protons (Figure S7 and Experimental Section). The aromatic substituent on the pyrrol-2(5*H*)-one cycle, the fragment from the substituted benzaldehydes, has several characteristic proton signals. Their number and coupling pattern depend on the number and position of the substituents in the starting benzaldehydes. For example, para-substituted benzaldehyde fragments are recognized after the two doublets with the roof-effect pattern, resonating in the interval 6.90−7.90 ppm. The only exception is the 4-fluoroaryl fragment (**2**), which is characterized by a triplet (at 7.15 ppm, H ortho to ^{19}F) and doublet of doublets (at 7.37 ppm, H meta to ^{19}F) due to proton−fluorine couplings (Figures S2 and S3). Protons from disubstituted benzaldehyde fragments have resonance signals either as two singlets with 1:2 integrals ratio (**5** with identical substituents CF_3; Experimental Section and Figure S3) or as a "small" doublet (2 Hz coupling constant), "big" doublet (8 Hz coupling constant), and doublet of doublets when substituents are in positions 2 and 5 or 3 and 4 (**11**, **13**, **14**, **15**, and **17**; Experimental Section and Figure S4). The protons from the amine and amide groups resonate as distinct singlets at the following chemical shifts: 7.18 ppm of NH_2 from the 3-((4-sulfonamidophenyl)amino) fragment, 7.27 ppm of NH_2 from the 1-((4-sulfonamidophenyl)amino) fragment, and around 8.70 ppm for the NH group. The differentiation between the two amido groups was obtained from the three-bond distance amido-protons correlation with quaternary carbon, present in the long-range HMBC spectra (Experimental Section and Figure S3).

A major source of information for the signal assignments in ^{13}C NMR spectra was data from two-dimensional proton−carbon correlation investigations. Because of the direct proton−carbon correlations found in HSQC spectra, protonated carbons could thus be easily identified, whereas quaternary carbons were assigned based on 2 or 3 bonds correlation signals from long-range HMBC spectra. A particular NMR profile was obtained for fluorine-containing compounds (**2**, **4**, and **5**; Experimental Section and Figure S3). Due to carbon−fluorine couplings, the carbon signals for 4-fluorophenyl, 4-(trifluoromethyl)phenyl, and 3,5-bis-(trifluoromethyl)phenyl fragments were assigned mainly from their specific shapes (Figure S3). Two cases were encountered: doublets at 115.7 ($^2J_{C,F}$ = 22 Hz, ortho-C), 129.0 ($^3J_{C,F}$ = 8 Hz, *meta*-C), 133.2 ($^4J_{C,F}$ = 3 Hz, *para*-C), and 161.7 ($^1J_{C,F}$ = 244 Hz, α-C) for 4-fluorophenyl and quartets at 123.9 ($^1J_{C,F}$ = 272 Hz, CF_3), 125.9 ($^3J_{C,F}$ = 4 Hz, ortho-C), and 128.6 ($^2J_{C,F}$ = 32 Hz, α-C) for the (trifluoromethyl)phenyl fragment. Long-range proton−carbon correlations were also used to obtain additional proof for the position of the substituent on the pyrrol-2(5*H*)-one cycle (Experimental Section and Figures S1−S6). Thus, the presence of the 4-sulfonamidophenyl-amino fragment in position 3 was confirmed by the existence of a correlation signal between the NH proton (at 8.70 ppm) and the carbonyl carbon (at 166.5 ppm). The protons from the benzaldehyde fragment showed three-bond correlation signals with aliphatic carbon C5 (approximately 62 ppm) supporting the proposed position for this fragment on the pyrrol-2(5*H*)-one cycle.

Chemical shift values for nitrogen atoms were obtained from the long-range ^1H,^{15}N-HMBC experiments (Experimental Section and Figure S3) based on the interactions with neighboring protons. Throughout the series, amine nitrogen resonates between 86 and 90 ppm, the two amide nitrogen atoms were observed around 96 ppm, whereas pyrrole nitrogen had the resonance signal between 140 and 145 ppm.

The chemical structure for the side reaction product **12** was deduced from 1D and 2D NMR spectra (Experimental Section

https://doi.org/10.1021/acs.jmedchem.3c02190
J. Med. Chem. 2024, 67, 3018−3038

Scheme 2. Doebner-Type Synthesis of Quinoline from Anilines, Reported by Weber et al.[46]

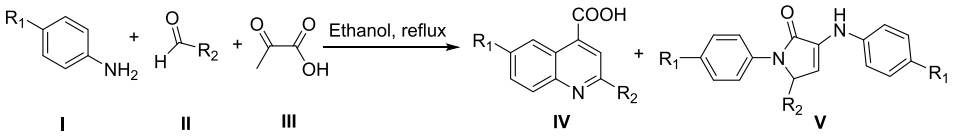

Scheme 3. Simplified Proposed Reaction Mechanism for the Reaction of Para-Amino Sulfonamide (I) with Aldehyde Derivatives (from the Aromatic, Aliphatic, or Cyclic Aldehyde Class) and Pyruvic Acid in Ethanol with Trifluoroacetic Acid in a Catalytic Amount

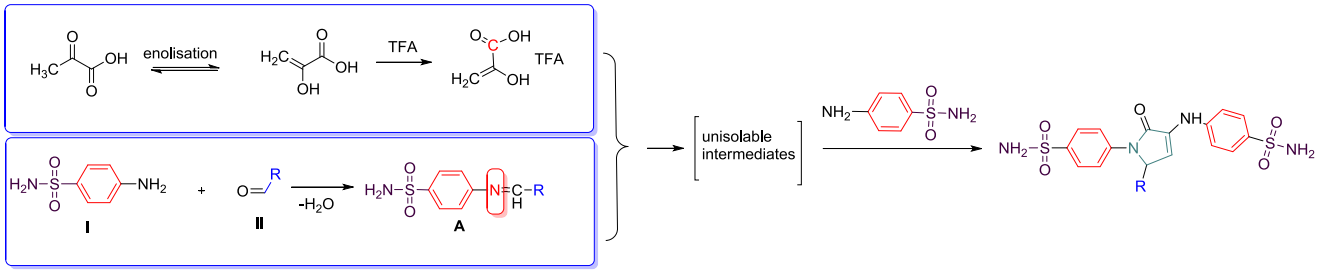

and Figure S8). Compared with the proton spectra obtained for the rest of the series, the main difference immediately observed was the presence of only one 4-sulfonamidophenyl fragment. As the signal for amine proton was still present (NH at 8.80 ppm) and the three-bond correlation signal in the HMBC spectrum with aromatic CH confirmed its covalent bond with the sulfonamidophenyl fragment, we deduced that the missing substituent was that from position 1. Additional information was obtained from the ^{13}C NMR spectrum and $^{1}H,^{15}N$-HMBC spectrum (Experimental Section and Figure S8). A significant deshielding of about 15 ppm (from approximately 62 to 76.8 ppm) was observed in the ^{13}C NMR spectrum for previously assigned CH-5 carbon from the pyrrol-2(5*H*)-one cycle. This shift toward a region characterized by carbon−oxygen bonds suggested that significant changes in the pyrrole cycle had occurred. Going further with NMR investigations, we recorded a long-range $^{1}H,^{15}N$-HMBC spectrum (Experimental Section and Figure S8) in which no signals for previously detected pyrrole nitrogen were obtained. This information, corroborated by MS analysis (Experimental Section and Figure S8), prompted us toward the proposed structure for side reaction product **12**, with the furan-2(5*H*)-one cycle instead of the pyrrol-2(5*H*)-one cycle.

The IR spectra of pyrrol-2-one compounds showed absorption bands between 3300 and 2900 cm^{-1} specific for aromatic and aliphatic C−H bonds, which proved the presence of the pyrrol-2-one heterocycle and phenyl cycle. The bands above 3300 cm^{-1} were caused by NH bonds, and in some cases by OH or OCH_3 groups, depending on the structure of the studied compound. The bands that were specific to C−N stretching bonds were in the range 2400−2300 cm^{-1}, and the bands that were specific to ketone carbonyl group absorption were in the range 1700−1650 cm^{-1}. Finally, the domain of 500−1600 cm^{-1} bands corresponded to the rest of the bonds present in the given structure.

Particularly, in the case of compound **12**, the 2-oxo-2,5-dihydrofuran presence in the molecule can be highlighted by the absorption band at 1751 cm^{-1} specific for this heterocycle ring ester. For compounds **20** and **21**, which have either a furan or a piperonal moiety, FT-IR spectra showed specific absorption bands in the ranges 1610−1560 and 1510−1475 cm^{-1}. All of the other absorption bands were in good agreement with the proposed structures.

MALDI-MS analysis was also used to confirm the reaction between *para*-amino sulfonamide, aldehyde derivatives, and pyruvic acid. Since the molecular ion occurred in the positive mode, only positive ions were examined. A good correlation between the estimated mass and the experimental ones was found for each compound (Experimental Section and Figures S1−S8). Thus, the MALDI-MS method validated all hypothesized structures for compounds **1**−**23**.

The proposed reaction mechanism for obtaining the compounds by reacting *para*-amino sulfonamide with aldehyde derivatives (from the aromatic, aliphatic, or cyclic aldehyde class) and pyruvic acid in ethanol with trifluoroacetic acid, in a catalytic amount, was in correlation with that proposed by Weber et al.[46] who reported that 3-arylamino-dihydro-pyrrol-2-ones were produced via the interaction of anilines with different aldehydes and pyruvic acid derivatives in the Doebner-type synthesis of quinoline **V** as well as the anticipated substituted quinoline-4-carboxylic acids **IV** (three-component product) (Scheme 2). Weber's group showed that the starting amine led to the formation of two major compounds: carboxyquinolines when the starting amine possessed electron-donating groups or pyrrol-2-one derivatives when the starting amine exhibited a withdrawing effect along with a side product from the reaction with carboxyquinolines as a major compound.

Thus, in our case, the sulfonamide moiety has a strong withdrawing effect, resulting in pyrrol-2-one derivatives as the principal product. To obtain pyrrol-2-one derivatives starting from a substituted aromatic amine (withdrawing effect), aldehydes, and pyruvic acid, the most probable "reaction mechanism" proceeds through the intermediate formation of an unstable imine compound, formed in the reaction between the aldehyde and amine groups. Once the reaction continued, the pyrrole derivatives were obtained (Scheme 3).

In order to predict the most favorable site for an electrophilic attack in compound A, with the imine group (Scheme 3), we performed quantum mechanical calculations—density functional theory calculations (DFT)[47] and condensed Fukui function analysis[48]—as described in the Experimental Section. In this goal, we calculated the Fukui

https://doi.org/10.1021/acs.jmedchem.3c02190
J. Med. Chem. 2024, 67, 3018−3038

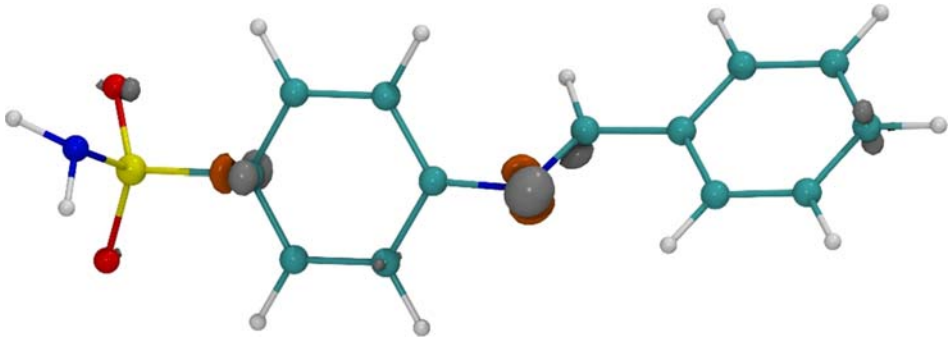

Figure 3. Representation of the Fukui function f^- of the imine general structure A, isodensity level 0.01. Nitrogen (blue), oxygen (red), sulfur (yellow), carbon (cyan), hydrogen (white), and Fukui function f^- (gray/orange).

Table 1. Inhibition Data of Human CA Isoforms I, II, IX, and XII with Compounds 1−16 and 19−21 (nM) and AAZ by a Stopped-Flow CO_2 Hydrase Assay[49]

	K_i (nM)[a]				
compd	hCA I	hCA II	hCA IX	hCA XII	selectivity index $\frac{K_i hCA\ II}{K_i hCA\ IX}$
1	52.7 ± 4.4	7.4 ± 0.5	26.1 ± 2.0	16.8 ± 1.0	0.28
2	96.7 ± 6.3	23.3 ± 1.4	29.4 ± 2.8	93.9 ± 9.3	0.79
3	293.5 ± 20.5	57.8 ± 4.4	18.4 ± 1.5	91.5 ± 9.1	3.14
4	80.7 ± 6.7	9.1 ± 0.5	168.6 ± 16.7	38.0 ± 2.2	0.05
5	12.3 ± 1.1	4.4 ± 0.3	39.7 ± 3.2	74.2 ± 6.6	0.11
6	53.6 ± 4.3	9.4 ± 0.7	25.7 ± 1.7	74.5 ± 6.5	0.36
7	237.5 ± 16.2	93.9 ± 8.5	23.9 ± 1.8	61.9 ± 4.9	3.92
8	870.9 ± 51.7	397.4 ± 23.7	30.6 ± 2.2	9.2 ± 0.5	12.98
9	604.8 ± 54.4	333.6 ± 25.3	1.9 ± 0.2	6.7 ± 0.3	175.57
10	51.1 ± 3.1	6.0 ± 0.4	10.8 ± 1.0	74.5 ± 3.8	0.55
11	41.5 ± 3.3	9.2 ± 0.7	2.9 ± 0.2	65.9 ± 4.6	3.17
12	357.5 ± 24.8	188.5 ± 16.6	1.8 ± 0.1	36.5 ± 2.0	104.72
13	45.5 ± 2.6	6.8 ± 0.4	3.4 ± 0.2	47.0 ± 3.8	2
14	3.9 ± 0.2	6.9 ± 0.6	3.2 ± 0.3	17.1 ± 1.6	2.15
15	34.9 ± 2.7	7.0 ± 0.5	2.4 ± 0.2	63.9 ± 5.2	2.91
16	36.9 ± 3.1	6.1 ± 0.3	3.7 ± 0.3	20.1 ± 1.6	1.64
19	416.4 ± 25.4	158.0 ± 11.6	211.3 ± 13.2	8.5 ± 0.8	0.74
20	46.9 ± 2.9	6.4 ± 0.5	25.8 ± 2.3	5.9 ± 0.6	0.24
21	95.5 ± 6.1	15.8 ± 1.2	150.4 ± 9.5	8.1 ± 0.8	0.10
AAZ	250.0 ± 21.0	12.1 ± 1.0	25.8 ± 2.5	5.7 ± 0.5	0.46

[a]Mean from three different assays, by a stopped-flow technique (errors were in the range of ±5−10% of the reported values).

function f^- (as shown in Figures 3, S9 and Table S1), and it was determined that the N4 nitrogen atom involved in the imine group was the most favored site for electrophilic attack. Next, we suppose the formation of unstable intermediates between the imine and pyruvic acid, followed by cyclization and addition of a new *p*-amino sulfonamide molecule resulted in a stable pyrrol-2-one compound.

Carbonic Anhydrase Inhibition. Compounds **1**−**16** and **19**−**21** were tested *in vitro* against the physiologically most relevant hCA isoforms such as I, II, IX, and XII by applying the stopped-flow technique and were compared in Table 1 with the standard sulfonamide inhibitor acetazolamide (**AAZ**).

From the inhibition data, we can draw the following structure−activity relationships (SARs):

—The cytosolic hCA I, which is widely expressed, was inhibited by all series at concentrations ranging from low nanomolar (K_I 3.9 nM for **14**) to high nanomolar values (K_I 870.9 nM for **8**). It is interesting to note that halogen atoms in position 4 of phenyl ring are deleterious for the activity, especially bromine (**3**), which showed 5.5-fold less activity than derivative **1** (K_I 293.5 and 52.7 nM, respectively) without substituents. On the other hand, two CF_3 groups in positions 3 and 5 (**5**) increased the potency of inhibition 4-fold, with a K_I of 12.3 nM. The hydroxyl group was found to play an important role in the activity against this isoform; indeed, compound **14** was the most potent inhibitor with a K_I of 3.9 nM. When the hydroxyl was masked as a methoxyl group, as in the case of **11**, the potency decreased 10-fold. Bulky moieties in position 4 were observed to be deleterious for the activity, as seen in **7**, **8**, **9**, and **19**, where the potency decreased by 1 order of magnitude order.

—From a general perspective, the second widely expressed cytosolic hCA II was better inhibited than hCA I, sharing similar features such as the location of the halogen atom in position 4. Derivative **3** with a bromine atom was found to be less active than fluorine analogue **2** with K_I values of 57.8 and 23.3 nM, respectively. Compound **5** with two CF_3 groups was the most potent inhibitor against this isoform, with a value of 4.4 nM. The hydroxyl groups also played an important role in modulating the activity, leading to low nanomolar inhibition as

https://doi.org/10.1021/acs.jmedchem.3c02190
J. Med. Chem. 2024, 67, 3018−3038

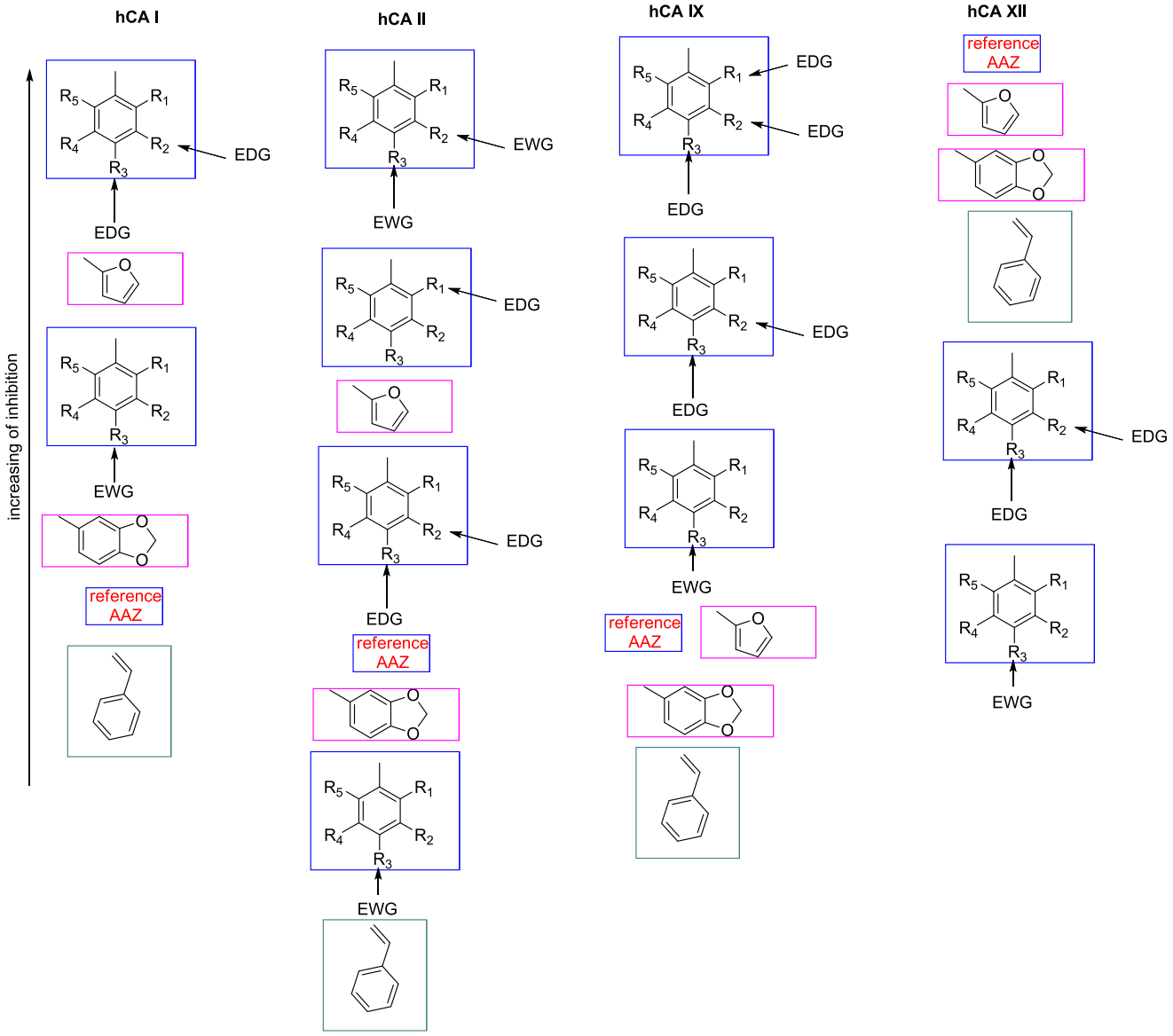

Figure 4. Schematic representation of the structure−activity relationship (SAR). EWG: electron-withdrawing group; EDG: electron-donating group.

observed in compounds **14** and **15**. On the other hand, when all of the hydroxyl groups were masked as methoxyl, a decrement of 27-fold in potency was observed. Similar to hCA I, bulky substituents in position 4 (**7** and **8**) were less active than the other derivatives in the series.

—All of the compounds in the series effectively inhibited the first tumor-associated hCA IX, with K_I values ranging from low nanomolar (1.9 nM for **9**) to medium nanomolar (211.2 nM for **19**). Unlike the cytosolic isoforms, this time, the bromine atom in position 4 (**3**) was observed to be more active than the fluorine analogues **2** or compound **1** without substituents (K_I 18.4, 29.4, and 26.1 nM, respectively). However, the CF_3 group in position 4 was found to be the least active among halogen derivatives, with a K_I of 168.6 nM. Interestingly, hydroxyl groups did not play a crucial role in the inhibition activity for this isoform because compound **12**, which had three methoxyl moieties, showed a K_I of 1.8 nM, making it the most potent inhibitor against hCA IX. As with the cytosolic isoforms, **19** with a bulkier moiety in position 4 was found to be deleterious for potency, with a K_I of 211.3 nM.

—The second tumor-associated hCA XII isoform was highly inhibited by the series tested, with K_I values in the low nanomolar range. Halogen atoms in position 4 were found to be detrimental to potency compared to **1** without substituents. In addition, as with hCA IX, hydroxyl groups did not play a role in modulating the activity. The replacement of the phenyl ring with a furan ring resulted in the best inhibitor against this isoform, with a K_I of 5.9 nM. Interestingly, the bulky moiety in position 4 enhanced the potency of the derivative, and compound **19** was found to be a potent and selective hCA XII inhibitor with a selectivity index of 8.5 compared with hCA II.

A schematic representation of the structure−activity relationship is presented in Figure 4.

X-ray Crystallographic Studies. Building upon the interesting findings from the CA inhibition experiments, we embarked on crystallographic studies focusing on a representative derivative, **12**, in complex with the hCA II isoform

https://doi.org/10.1021/acs.jmedchem.3c02190
J. Med. Chem. 2024, 67, 3018−3038

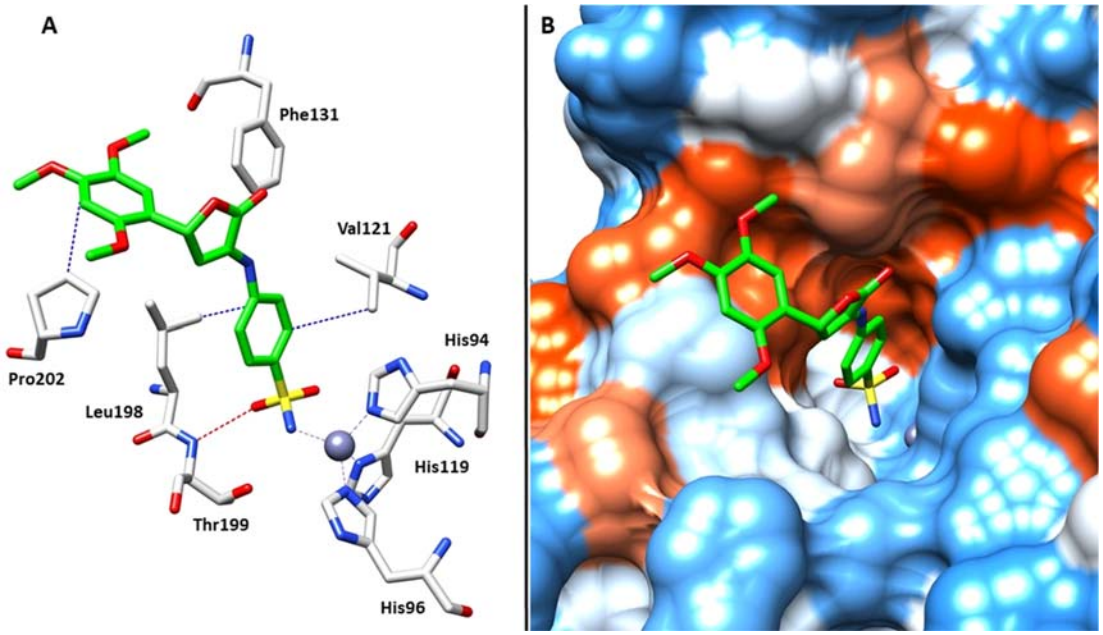

Figure 5. (A) X-ray crystal structures of hCA II bound with compound **12** (PDB: 8R2K). (B) Compound **12** inside the active site of hCA II. Hydrophobic (red) and hydrophilic (blue) residues are labeled. Residues involved in the binding of inhibitors are also shown; the gray sphere represents the zinc atom in the active site of the protein.

(Figure 5), in order to obtain an insight into ligand−protein interactions at the atomic level.

Analysis of the electron density (Figure S10) within the catalytic cleft confirmed the presence of ligand **12**. The sulfonamide moiety exhibited direct interaction with the zinc ion and formed a hydrogen bond with Thr199, aligning with the characteristic binding mode observed for this class of inhibitors.[50] Moreover, notable hydrophobic interactions emerged between the benzenesulfonamide moiety and the side chains of Val121 and Leu198, strengthening the stability of the complex within the active site (Figure 5A). Additionally, one hydrophobic interaction involving Pro202 was observed with the aromatic ring of the main scaffold. This interaction played a pivotal role in anchoring the ligand tail within the hydrophobic pocket of the active site, as illustrated in Figure 5B.

Docking Studies. Docking studies were applied to extend the X-ray crystallographic studies toward all of the investigated isoforms and explain the relationship between structural features and inhibition profiles of the most selective compounds **9** and **12** toward the tumor-associated isoforms hCA IX and XII (Tables 1 and 2). Given the stereocenter on carbon 5 in the five-ring central heterocycle, both (*R*)- and (*S*)-enantiomers of the selected compounds were investigated by docking to model the interactions they establish with the isoforms IX and XII of the hCA. For comparison, the studies were extended to the off-target hCA I and II.

Table 2. Docking Score of Ligands (*R*)-9, (*S*)-9, (*R*)-12, and (*S*)-12 in Complex with hCA I, II, IX, and XII

	docking score			
ligand	hCA I	hCA II	hCA IX	hCA XII
(*R*)-**9**	−6.087	−6.311	−7.579	−7.419
(*S*)-**9**	−4.159	−4.675	−6.438	−6.147
(*R*)-**12**	−5.376	−6.048	−7.312	−6.795
(*S*)-**12**	−5.285	−5.404	−6.743	−6.652

According to the literature,[51−54] all docking solutions found the benzenesulfonamide bound to the zinc ion in tetragonal coordination with the deprotonated nitrogen atom (SO_2NH^-). The stabilization of the ligands within the active sites is also supported by the formation of two H-bonds between the zinc-binder sulfonamide NH^- and S═O with the side chain OH and the backbone NH of T199, respectively. Moreover, the benzenesulfonamide aromatic ring is stabilized by van der Waals (vdW) interactions with residues A121/V121 (CA I/CA II, IX and XII), V143, L198, and W205.

In the hCA I active site, the (*R*)-**9** enantiomer oriented the benzenesulfonamide tail toward the polar pocket lined by W5, Y20, H200, and P201 engaging a H-bond with the S═O group and the side chain NH of W5. Instead, the *p*-phenoxy butyl pendant establishes vdW contacts with residues of the lipophilic part of the active site, that is with the residues F91, A121, L131, L141, V143, and V207 (Figure 6A). In (*S*)-**9**, the benzenesulfonamide tail is positioned in the same manner as in (*R*)-**9**. However, the inversion of the stereocenter on C5 moves the hydrophobic *p*-phenoxy butyl tail toward the polar region of the active site shaped by H64, H67, N69, and Q92. This makes the interaction between the two counterparts not optimal, despite the orientation of the butyl group toward V62 (Figure 6B). Compared to bulkier dual-tailed derivative **9**, the presence of a single tail on the furan-2-one ring allows both **12**-(*R*) and **12**-(*S*) enantiomers to better accommodate within the small hCA I active site (Figure 6C,D) and to the tail to establish a wide network of vdW interactions that stabilize the poses, thereby suggesting possible explanations about the better inhibitory activity of **12** versus **9** against hCA I.

In hCA II, the scenario is similar to that described in hCA I (Figure 6E−H). Again the interactions of (*R*)-**9** are more effective than those of (*S*)-**9** (Figure 6E, F) and the (*R*)- and (*S*)-**12** enantiomers fit more effectively within the hCA II

https://doi.org/10.1021/acs.jmedchem.3c02190
J. Med. Chem. 2024, 67, 3018−3038

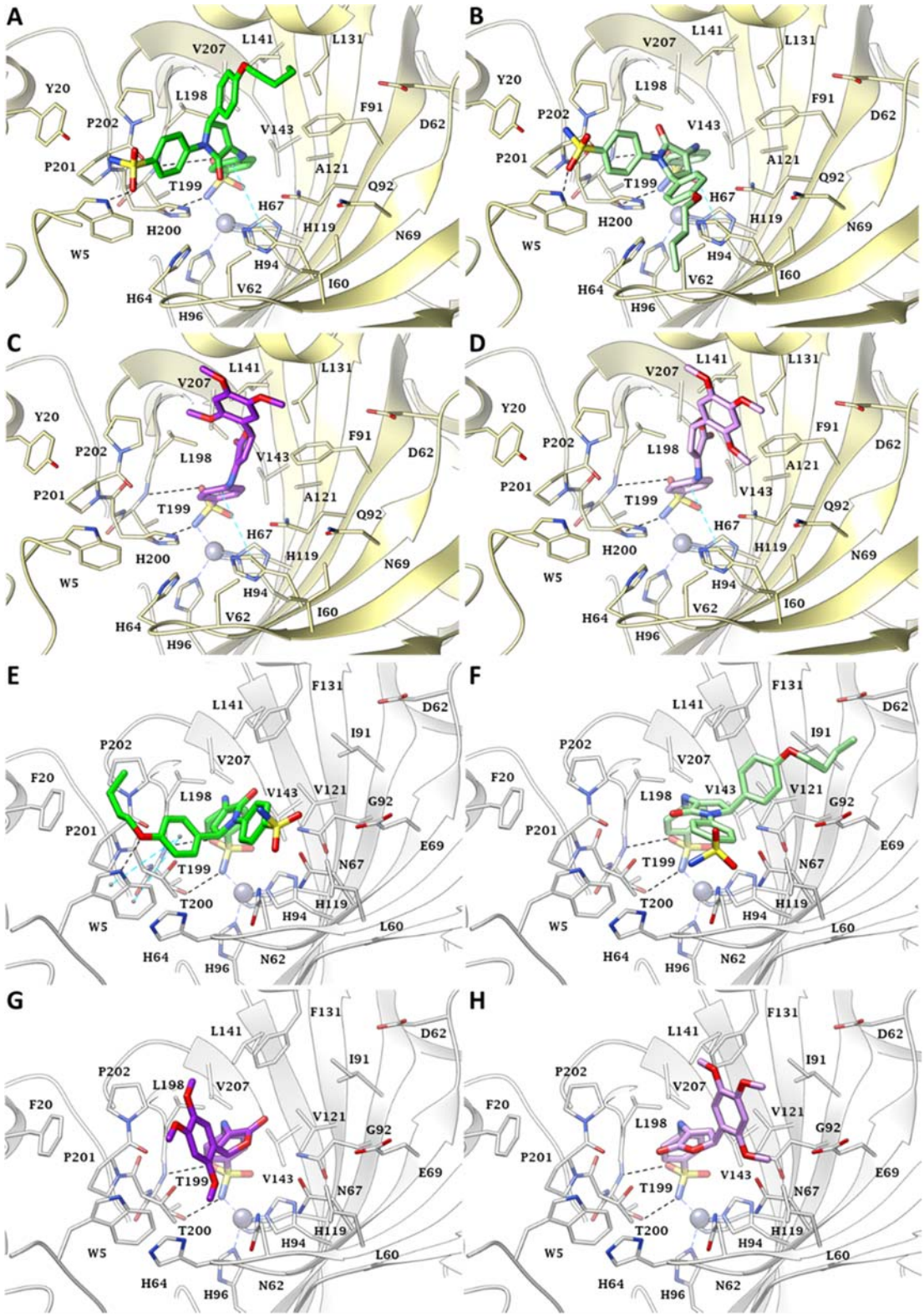

Figure 6. Predicted binding mode of ligands (*R*)-**9** (green), (*S*)-**9** (light-green), (*R*)-**12** (purple), (*S*)-**12** (light-purple) within the hCA I (PDB 2NMX; orange: (A−D)) and hCA II (PDB 3K34; white: (E−H)) active sites. H-bonds and $\pi-\pi$ stacking interactions are depicted as black and cyan dashed lines, respectively.

active site (Figure 6G,H). It is interesting to note the good agreement between the experimental and calculated solutions for ligand (*R*)-**12** (Figure 6G). The benzenesulfonamide pendant of both enantiomers of **9** is oriented toward the hydrophilic half of the active site lined by N62, H64, N67, E69, and G92. In (*R*)-**9**, the aromatic moiety of the *p*-phenoxy butyl tail engages $\pi-\pi$ stacking with the W5 residue and the same residue acts as a donor toward the ether oxygen atom of the

https://doi.org/10.1021/acs.jmedchem.3c02190
J. Med. Chem. 2024, 67, 3018−3038

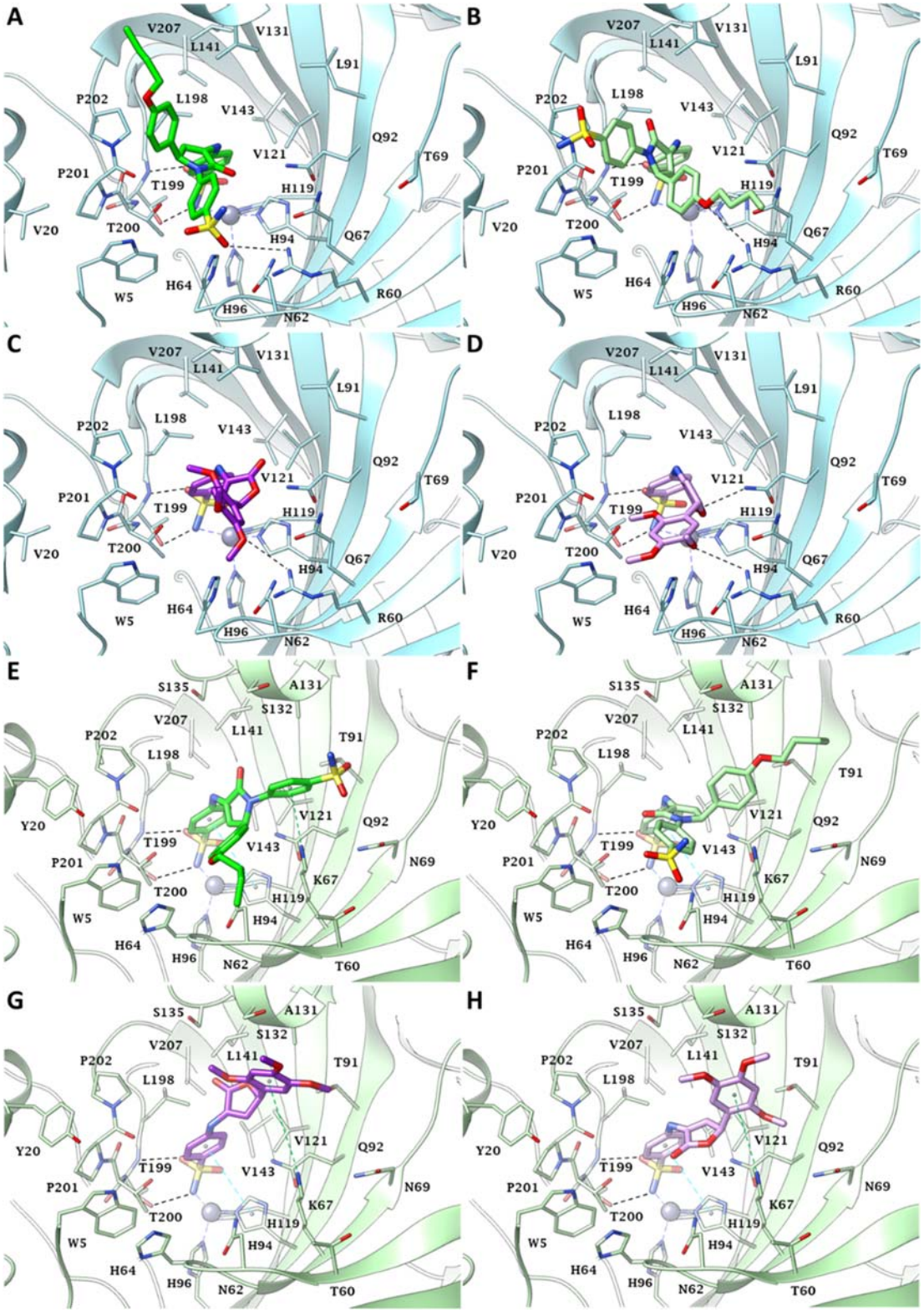

Figure 7. Predicted binding mode of ligands (*R*)-**9** (green), (*S*)-**9** (light-green), (*R*)-**12** (purple), (*S*)-**12** (light-purple) within the hCA IX (PDB 5FL4; blue: (A−D)) and hCA XII (PDB 1JDO; green: (E−H)) active sites. H-bonds and $\pi-\pi$ stacking interactions are depicted as black and cyan dashed lines, respectively.

ligand tail. Moreover, the butyl chain lodges in a region featured by hydrophobic residues, establishing interactions with the peculiar residue F20 (Figure 6E). On the other hand, (*S*)-**9** orients its *p*-phenoxy butyl tail on the opposite side of the active site where the butyl chain is flanked by the polar residues D62 and E69 (Figure 6F). The docking solutions within hCA IX show interactions with peculiar residues that could explain significant improvement in the inhibitory activity

https://doi.org/10.1021/acs.jmedchem.3c02190
J. Med. Chem. 2024, 67, 3018−3038

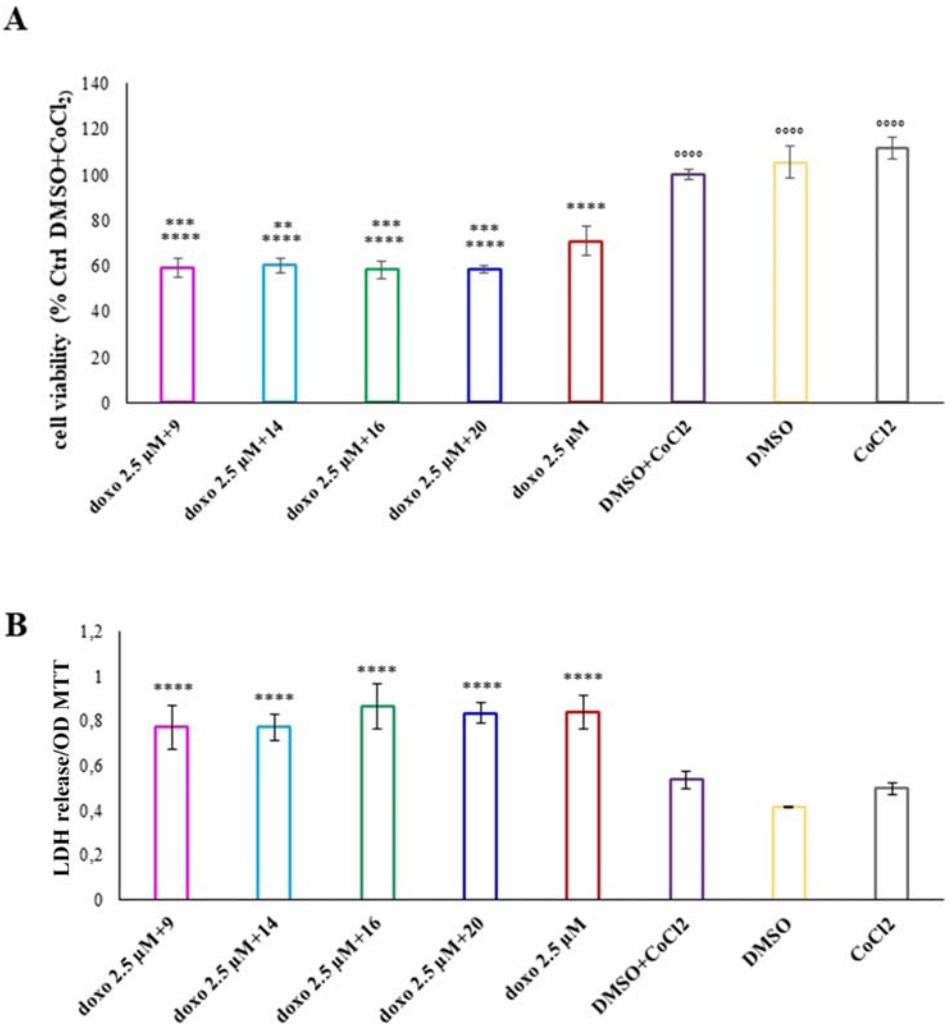

Figure 8. (A) MTT assay performed on MCF7 cells after 72 of treatment in the presence of doxo 2.5 μM or combinations of doxo 2.5 μM + compounds **9**, **14**, **16**, and **20** at 50 μM, under hypoxic conditions. Histogram represents the viability percentage of MCF7 normalized to control (cells exposed to DMSO+$CoCl_2$ 100 μM). Each bar of the histogram represents the mean of six biological replicates ± standard deviation. The most representative of three separate experiments is shown. **** vs DMSO+$CoCl_2$, $p < 0.0001$; *** vs doxo, $p < 0.001$; ** vs doxo, $p < 0.01$; °°°° vs doxo, $p < 0.0001$. (B) LDH cytotoxicity assay performed on MCF7 cells after 72 h of treatment in the presence of doxo 2.5 μM or combinations of doxo 2.5 μM + compounds **9**, **14**, **16**, and **20** at 50 μM, under hypoxic conditions. Histogram represents LDH leakage and is reported as OD 490 nm−OD 690 nm/OD MTT. Each bar of the histogram represents the mean of three biological replicates ± standard deviation. The most representative of three separate experiments is shown. **** vs DMSO+$CoCl_2$, $p < 0.0001$.

observed in the kinetic enzymatic assays for the compounds (Figure 7A−D). In detail, driven by the hydrogen bond formation between the sulfonamide S═O and the charged side chain guanidinium group of R60, the benzenesulfonamide tail of (*R*)-**9** orients toward the polar cleft lined by W5, R60, N62, H64, and Q67, positioning the *p*-phenoxy butyl pendant in the lipophilic half of the active site, which is defined V131, L141, P202, and V207 (Figure 7A). The inversion of the stereocenter in (*S*)-**9** causes the two pendants to swap their positions: the *p*-phenoxy butyl group lies toward the polar part of the binding pocket with the oxygen ether in H-bond distance with the charged side chain guanidinium group of R60. It is likely that the strength of this interaction is capable of counteracting the repulsions due to the polar nature of the surrounding environment (Figure 7B). Both enantiomers of **12** are involved in a H-bond between the exocyclic C═O of the furan-2-one ring and the side chain NH_2 of Q92, whereas the oxygen atom of *meta*-OCH_3 of the 2,4,5-trimethoxyphenyl tail is in H-bond distance with the side chain of R60 (Figure 7C,D). In particular, the improved inhibitory activity of compound **9** might come from its reduced steric hindrance within the hCA IX active site, which is roomier than those of hCA I and II. In addition, the described interactions involving the peculiar residue R60 stabilize the enantiomers of both **9** and **12** derivatives.

In hCA XII, the interaction with peculiar residues of this isoform with both ligands was observed (Figure 7E−H). The (*R*)-**9** isomer positions the benzenesulfonamide tail toward the polar residues K67, N69, T91, and Q92, undertaking a π−cation interaction between the benzene ring and the charged side chain of K67 and the *p*-phenoxy butyl pendant is located in the polar pocket lined by residues W5, T60, N62, H64, and K67 (Figure 7E). Instead, the (*S*)-**9** benzenesulfonamide group extends toward the residues W5, T60, N62, H64, and K67, while the *p*-phenoxy butyl tail spreads toward the N69 and T91 residues without establishing any characteristic inter-

https://doi.org/10.1021/acs.jmedchem.3c02190
J. Med. Chem. 2024, 67, 3018−3038

actions (Figure 7F). Thus, it is likely that the inhibition data toward this isoform, featured by a wider active site compared to the off-target hCA I and II, reflect the reduction in nonoptimal contacts of the compound, which are instead present in the other isoform active sites. The large cavity of hCA XII allows both enantiomers of **12** to arrange the 2,4,5-trimethoxyphenyl tail in the center region of the binding site. The tail is stabilized by aT-shaped π−cation interaction between the ligand benzene ring and the charged side chain of peculiar K67 (Figure 7G,H).

Even in the presence of inhibition data obtained on the racemic mixture of the derivatives under investigation, the docking results allow for some interesting concerns: (i) the (*R*)-enantiomer (that could be considered the "eutomer"), able to suitably arrange itself in the polar and apolar halves of the active sites, is preferred in the off-target isoforms hCA I and II. As discussed above, in the isoforms IX and XII, both enantiomers find a favorable place. The contribution of the (*S*)-"distomer" in these two CAs can therefore help to explain the better activity obtained from the inhibition tests.

(ii) Ligand **9**, designed according to the dual tail approach, is able to well suite into hCA IX and XII. The best fit of the compounds in the tumor-associated isoforms IX and XII is likely related to the ability of the tails to accommodate in the middle/outer rim of the active sites, engaging favorable interaction with peculiar residues of both isozymes.

(iii) In the roomier active site of the tumor-associated isoforms hCA IX and XII, ligand **12** is able to orient both enantiomers toward the peculiar residues R60 (hCA IX) and K67 (hCA XII), resulting in a better inhibition profile with respect to the off-target isoforms hCA I and II.

***In Vitro* Antiproliferative Activity.** Four compounds (**9**, **14**, **16**, and **20**) were chosen for their efficacy in the inhibition of the tumor-associated isoforms CA IX and CA XII. The effect of selected compounds was also tested on an *in vitro* tumoral biological model represented by MCF7 breast adenocarcinoma cell line. Nowadays, doxorubicin (doxo) represents the first-line drug in breast cancer therapeutic protocols, and for this reason, we aimed at evaluating the effect of a cotreatment of doxo and compounds **9**, **14**, **16**, and **20** on MCF7 metabolic activity, and, as a consequence, on cell viability. Doxo was administered at 2.5 μM concentration which is, according to previous studies published on this topic, a subtoxic dose able to keep a percentage of viable cells higher than 50%,[55] whereas the concentration chosen for compounds **9**, **14**, **16**, and **20** was 50 μM. Moreover, it is widely recognized that hCA IX and XII isoforms, responsible for severe events connected with tumor progression and bad prognosis, appear overexpressed in the presence of a hypoxic environment. As a consequence, in order to overexpress hCA IX and XII isoforms in MCF7 cells, before cotreaments of doxo 2.5 μM and compounds **9**, **14**, **16**, and **20**, a hypoxic condition was reproduced by administering cobalt(II) chloride hexahydrate ($CoCl_2$) at 100 μM for 48 h, chemically inducing HIF-1α, as already reported elsewhere.[56] Cotreatments of doxo 2.5 μM + compounds **9**, **14**, **16**, and **20** were kept up to 72 h; next, the metabolic activity was measured by the MTT test. The latter reveals that for both samples exposed to doxo 2.5 μM alone and to cotreatments of doxo 2.5 μM with compounds **9**, **14**, **16**, and **20** at 50 μM, a statistically significant reduction in cell metabolic activity is recorded with respect to cells exposed to DMSO+$CoCl_2$, assumed as control (Figure 8A).

The statistical analysis also discloses that MCF7 exposed to cotreatments of doxo 2.5 μM + compounds **9**, **14**, **16**, and **20** at 50 μM shows a further and significant reduction of metabolic activity compared to metabolic activity measured in the presence of doxo 2.5 μM alone. This data appeared particularly interesting as it underlines the capability of newly synthesized molecules to improve the performance of the first-line drug. strengthening its antitumoral activity thanks to the significant reduction of cancerous cell viability. After that, the cytotoxic effect of doxo 2.5 μM in combination with compounds **9**, **14**, **16**, and **20** at 50 μM on the MCF7 cell line was taken into consideration by measuring the release of lactate dehydrogenase (LDH) within the culture medium after 72 h of treatment under hypoxic conditions. The results of LDH assay reveal that, compared to control cells, all tested cotreatments are able to provoke a peak of cytotoxicity, increasing LDH spreading, in a statistically significant manner (Figure 8B), thus confirming the hypothesis that cotreatments of novel CA IX and XII inhibitors with doxo at a subtoxic dose could represent a strategic and innovative tool to counteract *in vitro* breast tumor growth. Moreover, this approach could strengthen the concept that CA IX/XII inhibitors can be added to well-established therapeutic protocols and that their combinations can limit the occurrence of side effects due to the dose reduction.

■ CONCLUSIONS

A one-pot, three-component procedure was used to produce new dihydro-pyrrol-2-one compounds with two sulfonamide moieties, with trifluoroacetic acid acting as a strong catalyst. To explore the correlation between the structure and reactivity of compound A (Scheme 3), its electronic structure was investigated using density functional theory calculations (DFT) and condensed Fukui function analysis, and it was determined that the nitrogen atom involved in the imine group is the most favored site for electrophilic attack.

The resulting compounds were examined in comparison to four human carbonic anhydrase isoforms (hCA I, hCA II, hCA IX, and hCA XII). The cytosolic hCA I, which is extensively expressed, was inhibited by all series at doses ranging from low nanomolar (K_I 3.9 nM for **14**) to high nanomolar values (K_I 870.9 nM for **8**). The second most abundantly expressed cytosolic hCA II was more effectively inhibited than hCA I, with K_I values ranging from low nanomolar for **9** (1.9 nM) to medium nanomolar for **19** (211.2 nM). All of the tested drugs in the series efficiently inhibited the first tumor-associated hCA IX, while the second tumor-associated hCA XII was also inhibited in good range. These issues are further and positively supported by biological evaluations performed on a breast cancer cell line in which the efficacy of a cotreatment on the viability of cancerous cells is evidenced, thus allowing the possibility to develop therapeutic protocols adopting reduced concentrations of the first-line drug, limiting, in parallel, doxorubicin-related side effects.

■ EXPERIMENTAL SECTION

Chemistry. Analytical thin-layer chromatography was performed with commercial silica gel plates 60 F254 (Merck Darmstadt, Germany) and visualized with UV light (λ_{max} = 254 or 365 nm). The NMR spectra included in this study were recorded on Bruker Avance NEO 400 and 600 MHz spectrometers equipped with 5 mm four nuclei direct detection *z*-gradient probe (H,C,F,Si-QNP) and 5 mm inverse detection multinuclear *z*-gradient probe, respectively.

https://doi.org/10.1021/acs.jmedchem.3c02190
J. Med. Chem. 2024, 67, 3018−3038

Proton and carbon chemical shifts are reported in δ units (ppm) relative to the residual solvent signal (ref: DMSO-d_6 ^{1}H, 2.51 ppm and ^{13}C, 39.47 ppm). H,H-COSY, H,C-HSQC, and H,C-HMBC experiments were recorded using standard pulse sequences as delivered by Bruker with a TopSpin 4.0.8 spectrometer control and processing software. The ^{15}N chemical shifts were obtained as projections from the 2D indirectly detected H,N-HMBC spectra and are referred to external liquid ammonia (0.0 ppm) using as external standard nitromethane (380.2 ppm). IR spectra were recorded on a Shimadzu IRTracer-100 instrument (Shimadzu U.S.A. Manufacturing, Inc., Canby, OR). The melting point of the compounds was measured on a MEL-TEMP capillary melting point apparatus from ambient temperature up to 400 °C. All commercially available products were used without further purification unless otherwise specified.

MALDI-MS. Mass spectra were acquired on a Bruker RapifleX MALDI-TOF/TOF (Bruker Daltonics, Bremen—Germany) equipped with a Smartbeam 3D laser. The FlexControl Version 4.0 and FlexAnalysis Version 4.0 software (Bruker, Bremen, Germany) were used to control the instrument and process the MS spectra. The samples were dissolved in DMSO and then diluted 10 times in methanol. For the MALDI matrix solutions, 20 mg of α-cyano-4-hydroxycinnamic acid (HCCA) was dissolved in 1 mL of methanol. Then, MALDI matrix solution and sample solution were mixed with each other in 1:1, 2:1, and 4:1 ratio, and finally 1 μL from each final solution was deposited onto the MALDI target and dried at room temperature prior to MALDI-MS analysis. Mass calibration of MALDI-TOF/TOF-MS was performed by the peptide mixture standard solution (Bruker Daltonics, Bremen—Germany). FlexControl 4.0 was used to optimize and acquire data using the following parameters: positive ion polarity in reflector mode, mass scan range (m/z 100−1600 Da), digitizer 1.25 GHz, detector voltage 2117 V, 1000 shots per pixel, and 5 kHz laser frequency. The laser power was set at 60−80% of the maximum and 1000 laser shots were accumulated for each spectrum.

General Procedure for the Synthesis of Compounds ***1*****−****23****.* In a 4 mL amount of ethanol, proper benzaldehyde (1 mmol) was combined with 1 mmol 4-aminobenzenesulfonamide. The reaction mixture was stirred at room temperature for 20 min. Trifluoracetic acid (20 μL) and pyruvic acid (1.5 mmol) in ethanol were then added to the mixture, which was then allowed to reflux for 12 h at a catalytic rate. By removing the resultant suspension and washing the solid with ethanol, the necessary compound was produced. To aid in recrystallization, dichloromethane and ethanol were utilized. The high-performance liquid chromatography (HPLC) analysis conditions were as follows: column: XDB-C18 (100 mm × 4.6 mm); mobile phase: ultrapure water (containing 0.1%% formic acid), 20%/80% ultrapure water/acetonitrile solution (0.1% formic acid); wavelength: 280 nm; rate: 1 mL/min. All compounds were of >95% purity as determined by HPLC. Spectra for representative compounds are displayed in the Supporting Information.

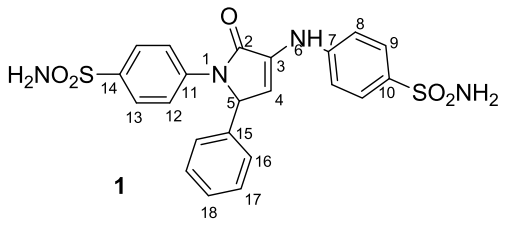

1-(4-Sulfamoylphenyl)-3-((4-sulfamoylphenyl)amino)-5-phenyl-1H-pyrrol-2(5H)-one ***1****.* Yellow solid; 79% yield; mp 211−213 °C; IR ATR ν (cm^{-1}): 3672, 2978, 2900, 2360, 1678, 1600, 1539, 1377, 1327, 1153, 1068, 1012, 895, 536. ^{1}H NMR (DMSO-d_6, 400.1 MHz, δ (ppm)): 6.19 (1H, d, ^3J = 3 Hz, H-5), 6.66 (1H, d, ^3J = 3 Hz, H-4), 7.17 (2H, s, NH_2-10), 7.24−7.26 (3H, m, NH_2 and H-18), 7.31−7.32 (4H, m, H-16 and H-17), 7.44 (2H, d, ^3J = 9 Hz, H-8), 7.69 (2H, d, ^3J = 9 Hz, H-9), 7.76 (2H, d, ^3J = 9 Hz, H-13), 7.85 (2H, d, ^3J = 9 Hz, H-12), 8.68 (1H, s, NH). ^{13}C NMR (DMSO-d_6, 100.6 MHz, δ (ppm)): 62.3 (CH-5), 113.2 (CH-4), 115.9 (CH-8), 120.9 (CH-12), 126.4 (CH-13), 126.8 (CH-16), 127.0 (CH-9), 128.0 (CH-18), 128.9 (CH-17), 130.9 (C-3), 135.2 (C-10), 137.1 (C-15), 139.4 (C-14), 139.7 (C-11), 144.8 (C-7), 166.5 (CO-2). ^{15}N NMR (DMSO-d_6, 40.5 MHz, δ (ppm)): 89.5 (NH), 96.4 (2×NH_2), 142.9 (N). HRMS (MALDI-TOF/TOF) m/z calcd for $[M + H]^+$, 485.09087; found, 485.07474.

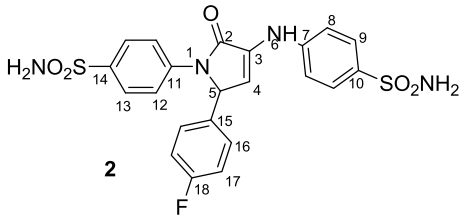

5-(4-Fluorophenyl)-1-(4-sulfamoylphenyl)-3-((4-sulfamoylphenyl)amino)-1H-pyrrol-2(5H)-one ***2****.* Yellow solid; 63% yield; mp 257−258 °C; IR ATR ν (cm^{-1}): 3672, 3371, 3317, 3267, 2981, 2900, 2360, 1685, 1651, 1593, 1504, 1392, 1338, 1307, 1227, 1146, 1076, 894, 821, 651, 540. ^{1}H NMR (DMSO-d_6, 400.1 MHz, δ (ppm)): 6.22 (1H, d, ^3J = 3 Hz, H-5), 6.65 (1H, d, ^3J = 3 Hz, H-4), 7.15 (2H, t, $^3J_{H,H}$ = $^3J_{H,F}$ = 9 Hz, H-17), 7.18 (2H, s, NH_2-10), 7.28 (2H, s, NH_2-14), 7.37 (2H, dd, $^3J_{H,H}$ = 9 Hz, $^4J_{H,F}$ = 5 Hz H-16), 7.45 (2H, d, ^3J = 9 Hz, H-8), 7.70 (2H, d, ^3J = 9 Hz, H-9), 7.77 (2H, d, ^3J = 9 Hz, H-13), 7.84 (2H, d, ^3J = 9 Hz, H-12), 8.70 (1H, s, NH). ^{13}C NMR (DMSO-d_6, 100.6 MHz, δ (ppm)): 61.6 (CH-5), 112.9 (CH-4), 115.7 (d, $^2J_{C,F}$ = 22 Hz, CH-17), 116.0 (CH-8), 121.0 (CH-12), 126.4 (CH-13), 127.0 (CH-9), 129.0 (d, $^3J_{C,F}$ = 8 Hz, CH-16), 131.1 (C-3), 133.2 (d, $^4J_{C,F}$ = 3 Hz, C-15), 135.2 (C-10), 139.5 (C-14), 139.6 (C-11), 144.8 (C-7), 161.7 (d, $^1J_{C,F}$ = 244 Hz, C-18), 166.4 (CO-2). ^{19}F NMR (DMSO-d_6, 376.4 MHz, δ (ppm)): −113.9. ^{15}N NMR (DMSO-d_6, 60.8 MHz, δ (ppm)): 89.1 (NH), 95.6 (2×NH_2), 143.4 (N). HRMS (MALDI-TOF/TOF) m/z calcd for $[M + H]^+$, 503.08144; found, 503.07774.

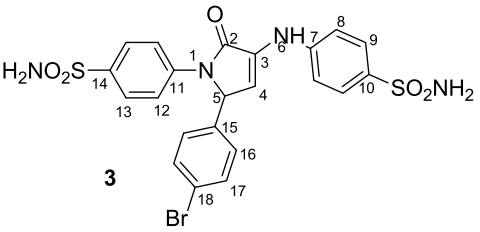

5-(4-Bromophenyl)-1-(4-sulfamoylphenyl)-3-((4-sulfamoylphenyl)amino)-1H-pyrrol-2(5H)-one ***3****.* Yellow solid; 82% yield; mp 237−239 °C; IR ATR ν (cm^{-1}): 3676, 3371, 3317, 3267, 2974, 2901, 2359, 1685, 1651, 1597, 1535, 1504, 1404, 1381, 1338, 1307, 1157, 1072, 898, 825, 652, 540. ^{1}H NMR (DMSO-d_6, 400.1 MHz, δ (ppm)): 6.20 (1H, d, ^3J = 3 Hz, H-5), 6.65 (1H, d, ^3J = 3 Hz, H-4), 7.17 (2H, s, NH_2-10), 7.26 (2H, s, NH_2-14), 7.29 (2H, d, ^3J = 9 Hz, H-16), 7.44 (2H, d, ^3J = 9 Hz, H-8), 7.52 (2H, d, ^3J = 9 Hz, H-17), 7.69 (2H, d, ^3J = 9 Hz, H-9), 7.77 (2H, d, ^3J = 9 Hz, H-13), 7.83 (2H, d, ^3J = 9 Hz, H-12), 8.71 (1H, s, NH). ^{13}C NMR (DMSO-d_6, 100.6 MHz, δ (ppm)): 61.6 (CH-5), 112.6 (CH-4), 116.0 (CH-8), 120.9 (CH-12), 121.1 (C-18), 126.4 (CH-13), 127.0 (CH-9), 129.2 (CH-16), 131.2 (C-3), 131.8 (CH-17), 135.2 (C-10), 136.6 (C-15), 139.4 (C-14), 139.5 (C-11), 144.7 (C-7), 166.4 (CO-2). ^{15}N NMR (DMSO-d_6, 60.8 MHz, δ (ppm)): 89.5 (NH), 95.6 (2×NH_2), 142.8 (N). HRMS (MALDI-TOF/TOF) m/z calcd for $[M + H]^+$, 561.99598; found, 562.96950.

1-(4-Sulfamoylphenyl)-3-((4-sulfamoylphenyl)amino)-5-(4-(trifluoromethyl)phenyl)-1H-pyrrol-2(5H)-one ***4****.* White solid; 60% yield; mp 271−273 °C; IR ATR ν (cm^{-1}): 3676, 3313, 3263, 2974, 2901, 2361, 1681, 1651, 1597, 1539, 1381, 1327, 1153, 1103, 1068, 825, 651, 540. ^{1}H NMR (DMSO-d_6, 400.1 MHz, δ (ppm)): 6.33 (1H, d, ^3J = 3 Hz, H-5), 6.68 (1H, d, ^3J = 3 Hz, H-4), 7.17 (2H, s, NH_2-10), 7.26 (2H, s, NH_2-14), 7.44 (2H, d, ^3J = 9 Hz, H-8), 7.56 (2H, d, ^3J = 9 Hz, H-16), 7.68−7.71 (4H, m, H-9 and H-17), 7.77

https://doi.org/10.1021/acs.jmedchem.3c02190
J. Med. Chem. 2024, 67, 3018−3038

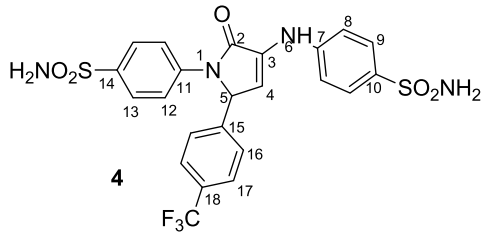

4

(2H, d, ^3J = 9 Hz, H-13), 7.86 (2H, d, ^3J = 9 Hz, H-12), 8.74 (1H, s, NH). ^{13}C NMR (DMSO-d_6, 100.6 MHz, δ (ppm)): 61.7 (CH-5), 112.3 (CH-4), 116.1 (CH-8), 120.8 (CH-12), 123.9 (q, $^1J_{C,F}$ = 272 Hz, CF_3), 125.9 (q, $^3J_{C,F}$ = 4 Hz, CH-17), 126.5 (CH-13), 127.0 (CH-9), 127.8 (CH-16), 128.6 (q, $^2J_{C,F}$ = 32 Hz, C-18), 131.3 (C-3), 135.3 (C-10), 139.5 (C-14), 139.6 (C-11), 142.2 (C-15), 144.7 (C-7), 166.4 (CO-2). ^{19}F NMR (DMSO-d_6, 376.4 MHz, δ (ppm)): −61.1. ^{15}N NMR (DMSO-d_6, 60.8 MHz, δ (ppm)): 89.2 (NH), 95.6 (2×NH_2), 142.2 (N). HRMS (MALDI-TOF/TOF) m/z calcd for $[M + H]^+$, 553.07825; found, 552.96527.

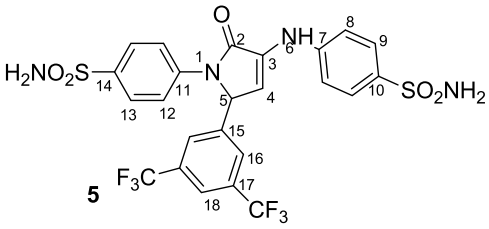

5

5-(3,5-Bis(trifluoromethyl)phenyl)-1-(4-sulfamoylphenyl)-3-((4-sulfamoylphenyl)amino)-1H-pyrrol-2(5H)-one ***5***. Yellow solid; 56% yield; mp 290−292 °C; IR ATR ν (cm^{-1}): 3675, 3310, 3262, 2971, 2900, 2360, 1680, 1653, 1596, 1535, 1384, 1326, 1150, 1101, 1064, 821, 650, 540. ^{1}H NMR (DMSO-d_6, 400.1 MHz, δ (ppm)): 6.46 (1H, d, ^3J = 3 Hz, H-5), 6.75 (1H, d, ^3J = 3 Hz, H-4), 7.18 (2H, s, NH_2-10), 7.29 (2H, s, NH_2-14), 7.46 (2H, d, ^3J = 9 Hz, H-8), 7.69 (2H, d, ^3J = 9 Hz, H-9), 7.79 (2H, d, ^3J = 9 Hz, H-13), 7.86 (2H, d, ^3J = 9 Hz, H-12), 8.02 (1H, s, H-18), 8.08 (2H, s, H-16), 8.78 (1H, s, NH). ^{13}C NMR (DMSO-d_6, 100.6 MHz, δ (ppm)): 61.1 (CH-5), 111.5 (CH-4), 116.1 (CH-8), 121.1 (CH-12), 122.1 (CH-18), 123.0 (q, $^1J_{C,F}$ = 272 Hz, CF_3), 126.6 (CH-13), 127.0 (CH-9), 128.0 (CH-16), 130.7 (q, $^2J_{C,F}$ = 33 Hz, C-17), 131.7 (C-3), 135.4 (C-10), 139.2 (C-11), 139.8 (C-14), 141.1 (C-15), 144.6 (C-7), 166.4 (CO-2). ^{19}F NMR (DMSO-d_6, 376.4 MHz, δ (ppm)): −61.2. ^{15}N NMR (DMSO-d_6, 60.8 MHz, δ (ppm)): 89.5 (NH), 95.6 (2×NH_2), 140.2 (N). HRMS (MALDI-TOF/TOF) m/z calcd for $[M + H]^+$, 621.06564; found, 620.91500.

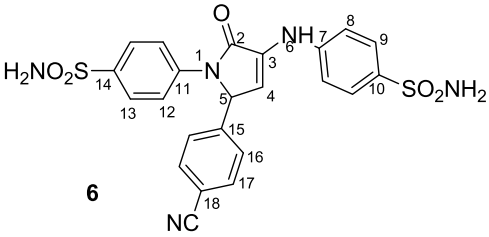

6

5-(4-Cyanophenyl)-1-(4-sulfamoylphenyl)-3-((4-sulfamoylphenyl)amino)-1H-pyrrol-2(5H)-one ***6***. Yellow solid; 80% yield; mp 230−231 °C; IR ATR ν (cm^{-1}): 3317, 3256, 2989, 2897, 2353, 2225, 1674, 1651, 1593, 1547, 1500, 1392, 1323, 1153, 1100, 910, 821, 648, 536. ^{1}H NMR (DMSO-d_6, 400.1 MHz, δ (ppm)): 6.32 (1H, d, ^3J = 3 Hz, H-5), 6.67 (1H, d, ^3J = 3 Hz, H-4), 7.18 (2H, s, NH_2-10), 7.28 (2H, s, NH_2-14), 7.44 (2H, d, ^3J = 9 Hz, H-8), 7.54 (2H, d, ^3J = 9 Hz, H-16), 7.69 (2H, d, ^3J = 9 Hz, H-9), 7.77 (2H, d, ^3J = 9 Hz, H-13), 7.80 (2H, d, ^3J = 9 Hz, H-17),7.84 (2H, d, ^3J = 9 Hz, H-12), 8.76 (1H, s, NH). ^{13}C NMR (DMSO-d_6, 100.6 MHz, δ (ppm)): 61.8 (CH-5), 110.8 (C-18), 111.9 (CH-4), 116.1 (CH-8), 118.4 (CN), 120.8 (CH-12), 126.5 (CH-13), 127.0 (CH-9), 127.9 (CH-16), 131.4 (C-3), 132.9 (CH-17), 135.4 (C-10), 139.4 (C-14), 139.6 (C-11), 143.1 (C-15), 144.6 (C-7), 166.4 (CO-2). ^{15}N NMR (DMSO-d_6, 60.8 MHz, δ (ppm)): 89.5 (NH), 95.6 (2×NH_2), 141.1 (N). HRMS (MALDI-TOF/TOF) m/z calcd for $[M + H]^+$, 510.08611; found, 510.92761.

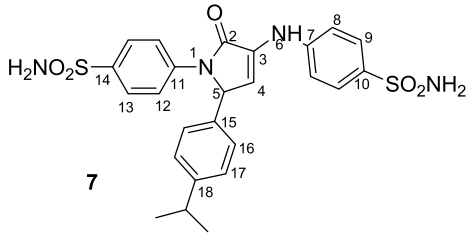

7

5-(4-Isopropylphenyl)-1-(4-sulfamoylphenyl)-3-((4-sulfamoylphenyl)amino)-1H-pyrrol-2(5H)-one ***7***. Yellow solid; 67% yield; mp 239−241 °C; IR ATR ν (cm^{-1}): 3672, 3309, 3267, 2970, 2904, 2360, 2337, 1678, 1651, 1593, 1543, 1500, 1392, 1327, 1257, 1145, 1083, 1053, 894, 821, 648, 536. ^{1}H NMR (DMSO-d_6, 400.1 MHz, δ (ppm)): 1.13 (3H, d, ^3J = 7 Hz, CH_3), 1.14 (3H, d, ^3J = 7 Hz, CH_3), 2.82 (1H, heptet, ^3J = 7 Hz, CH), 6.16 (1H, d, ^3J = 3 Hz, H-5), 6.64 (1H, d, ^3J = 3 Hz, H-4), 7.17 (2H, s, NH_2-10), 7.20 (2H, d, ^3J = 9 Hz, H-17), 7.23 (2H, d, ^3J = 9 Hz, H-16), 7.27 (2H, s, NH_2-14), 7.44 (2H, d, ^3J = 9 Hz, H-8), 7.69 (2H, d, ^3J = 9 Hz, H-9), 7.77 (2H, d, ^3J = 9 Hz, H-13), 7.86 (2H, d, ^3J = 9 Hz, H-12), 8.66 (1H, s, NH). ^{13}C NMR (DMSO-d_6, 100.6 MHz, δ (ppm)): 23.7 (2×CH_3), 32.9 (CH), 62.0 (CH-5), 113.4 (CH-4), 115.9 (CH-8), 120.9 (CH-12), 126.4 (CH-13), 126.8 and 126.9 (CH-16 and CH-17), 127.0 (CH-9), 130.8 (C-3), 134.3 (C-15), 135.1 (C-10), 139.4 (C-14), 139.7 (C-11), 144.8 (C-7), 148.1 (C-18), 166.5 (CO-2). ^{15}N NMR (DMSO-d_6, 60.8 MHz, δ (ppm)): 88.5 (NH), 95.6 (2×NH_2), 143.4 (N). HRMS (MALDI-TOF/TOF) m/z calcd for $[M + H]^+$, 527.13782; found, 527.07152.

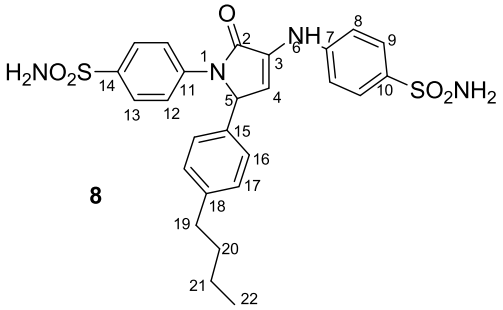

8

5-(4-Butylphenyl)-1-(4-sulfamoylphenyl)-3-((4-sulfamoylphenyl)amino)-1H-pyrrol-2(5H)-one ***8***. Yellow solid; 88% yield; mp 250−251 °C; IR ATR ν (cm^{-1}): 3676, 3363, 3305, 3248, 2982, 2904, 2360, 1670, 1647, 1597, 143, 1500, 1396, 1311, 1157, 1068, 910, 829, 682, 651, 570, 536. ^{1}H NMR (DMSO-d_6, 600.1 MHz, δ (ppm)): 0.86 (3H, t, ^3J = 7 Hz, CH_3), 1.26 (2H, sextet, ^3J = 7 Hz, CH_2−21), 1.48 (2H, quintet, ^3J = 7 Hz, CH_2−20), 2.7−2.49 (2H, m, CH_2−19 overlapped with DMSO), 6.15 (1H, d, ^3J = 3 Hz, H-5), 6.64 (1H, d, ^3J = 3 Hz, H-4), 7.13 (2H, d, ^3J = 9 Hz, H-17), 7.17 (2H, s, NH_2-10), 7.21 (2H, d, ^3J = 9 Hz, H-16), 7.26 (2H, s, NH_2-14), 7.43 (2H, d, ^3J = 9 Hz, H-8), 7.68 (2H, d, ^3J = 9 Hz, H-9), 7.76 (2H, d, ^3J = 9 Hz, H-13), 7.84 (2H, d, ^3J = 9 Hz, H-12), 8.66 (1H, s, NH). ^{13}C NMR (DMSO-d_6, 150.9 MHz, δ (ppm)): 13.7 (CH_3), 21.8 (CH_2−21), 32.9 (CH_2−20), 34.4 (CH_2−19), 62.1 (CH-5), 113.4 (CH-4), 115.9 (CH-8), 120.9 (CH-12), 126.4 (CH-13), 126.8 (CH-16), 127.0 (CH-9), 128.8 (CH-17), 130.8 (C-3), 134.2 (C-15), 135.1 (C-10), 139.4 (C-14), 139.7 (C-11), 142.2 (C-18), 144.9 (C-7), 158.4 (C-18), 166.5 (CO-2). ^{15}N NMR (DMSO-d_6, 60.8 MHz, δ (ppm)): 89.8 (NH), 96.4 (2×NH_2), 143.1 (N). HRMS (MALDI-TOF/TOF) m/z calcd for $[M + H]^+$, 541.15347; found, 541.03098.

5-(4-Butoxyphenyl)-1-(4-sulfamoylphenyl)-3-((4-sulfamoylphenyl)amino)-1H-pyrrol-2(5H)-one ***9***. Yellow solid; 85%

https://doi.org/10.1021/acs.jmedchem.3c02190
J. Med. Chem. 2024, 67, 3018−3038

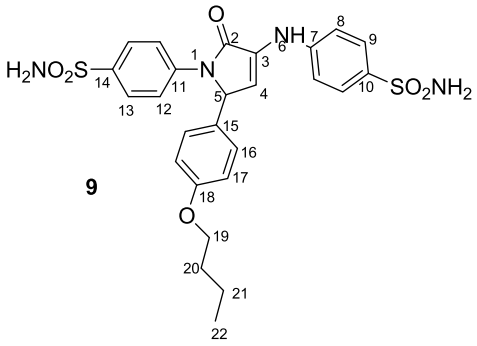

9

yield; mp 231−233 °C; IR ATR ν (cm^{-1}): 3672, 3356, 3302, 3259, 2978, 2904, 2356, 1681, 1654, 1593, 1539, 1512, 1381, 1303, 1253, 1153, 1072, 898, 825, 709, 570, 536. ^{1}H NMR (DMSO-d_6, 400.1 MHz, δ (ppm)): 0.89 (3H, t, ^3J = 7 Hz, CH_3), 1.39 (2H, sextet, ^3J = 7 Hz, CH_2−21), 1.64 (2H, quintet, ^3J = 7 Hz, CH_2−20), 3.89 (2H, t, ^3J = 7 Hz, CH_2−19), 6.13 (1H, d, ^3J = 2 Hz, H-5), 6.62 (1H, d, ^3J = 2 Hz, H-4), 6.85 (2H, d, ^3J = 9 Hz, H-17), 7.18 (2H, s, NH_2-10), 7.21 (2H, d, ^3J = 9 Hz, H-16), 7.27 (2H, s, NH_2-14), 7.44 (2H, d, ^3J = 9 Hz, H-8), 7.69 (2H, d, ^3J = 9 Hz, H-9), 7.76 (2H, d, ^3J = 9 Hz, H-13), 7.83 (2H, d, ^3J = 9 Hz, H-12), 8.66 (1H, s, NH). ^{13}C NMR (DMSO-d_6, 100.6 MHz, δ (ppm)): 13.6 (CH_3), 18.7 (CH_2−21), 30.7 (CH_2−20), 61.9 (CH-5), 67.0 (CH_2−19), 113.5 (CH-4), 114.7 (CH-17), 115.9 (CH-8), 121.0 (CH-12), 126.3 (CH-13), 127.0 (CH-9), 128.2 (CH-16), 128.4 (C-15), 130.8 (C-3), 135.1 (C-10), 139.3 (C-14), 139.7 (C-11), 144.9 (C-7), 158.4 (C-18), 166.4 (CO-2). ^{15}N NMR (DMSO-d_6, 60.8 MHz, δ (ppm)): 88.6 (NH), 95.8 (2×NH_2), 144.4 (N). HRMS (MALDI-TOF/TOF) m/z calcd for $[M + H]^+$, 557.14838; found, 557.03490.

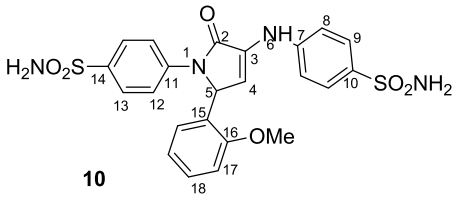

10

5-(2-Methoxyphenyl)-1-(4-sulfamoylphenyl)-3-((4-sulfamoylphenyl)amino)-1H-pyrrol-2(5H)-one ***10***. Yellow solid; 75% yield; mp 190−192 °C; IR ATR ν (cm^{-1}): 3668, 3325, 3248, 2970, 2897, 2360, 2330, 1681, 1651, 1593, 1531, 1493, 1373, 1330, 1246, 1157, 1099, 1049, 906, 825, 725, 540. ^{1}H NMR (DMSO-d_6, 400.1 MHz, δ (ppm)): 3.91 (3H, s, OCH_3-16), 6.37 (1H, d, ^3J = 2 Hz, H-5), 6.56 (1H, d, ^3J = 2 Hz, H-4), 6.83 (1H, t, ^3J = 8 Hz, H-19), 6.93 (1H, d, ^3J = 8 Hz, H-20), 7.07 (1H, d, ^3J = 8 Hz, H-17), 7.16 (2H, s, NH_2-10), 7.23 (1H, t, ^3J = 8 Hz, H-18), 7.27 (2H, s, NH_2-14), 7.42 (2H, d, ^3J = 9 Hz, H-8), 7.69 (2H, d, ^3J = 9 Hz, H-9), 7.77 (4H, bs, H-12 and H-12), 8.63 (1H, s, NH). ^{13}C NMR (DMSO-d_6, 100.6 MHz, δ (ppm)): 55.9 (OCH_3-16), 57.0 (CH-5), 111.7 (CH-17), 112.0 (CH-4), 115.9 (CH-8), 120.1 (CH-12), 120.9 (CH-19), 124.0 (C-15), 126.5 (CH-13), 126.6 (CH-20), 127.0 (CH-9), 129.3 (CH-18), 131.4 (C-3), 135.0 (C-10), 139.2 (C-14), 139.9 (C-11), 144.8 (C-7), 157.1 (C-16), 166.7 (C-2). ^{15}N NMR (DMSO-d_6, 40.5 MHz, δ (ppm)): 88.7 (NH), 95.2 (2×NH_2), 141.5 (N). HRMS (MALDI-TOF/TOF) m/z calcd for $[M + H]^+$, 515.10143; found, 514.97008.

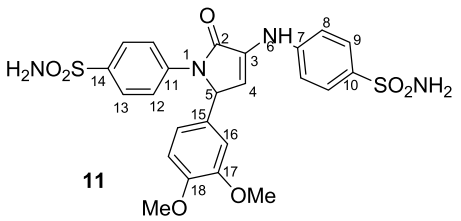

11

5-(3,4-Dimethoxyphenyl)-1-(4-sulfamoylphenyl)-3-((4-sulfamoylphenyl)amino)-1H-pyrrol-2(5H)-one ***11***. Yellow solid; 73% yield; mp 207−208 °C; IR ATR ν (cm^{-1}): 3672, 3360, 3271, 2970, 2904, 2360, 2338, 1693, 1663, 1593, 1539, 1516, 1377, 1323, 1303, 1261, 1145, 1049, 906, 817, 740, 652, 538. ^{1}H NMR (DMSO-d_6, 400.1 MHz, δ (ppm)): 3.68 (3H, s, CH_3-18), 3.71 (3H, s, CH_3-17), 6.11 (1H, d, ^3J = 3 Hz, H-5), 6.63 (1H, d, ^3J = 3 Hz, H-4), 6.80 (1H, dd, ^3J = 8 Hz, ^4J = 2 Hz, H-20), 6.88 (1H, d, ^3J = 8 Hz, H-19), 6.92 (1H, d, ^4J = 2 Hz, H-16), 7.18 (2H, s, NH_2-10), 7.27 (2H, s, NH_2-14), 7.44 (2H, d, ^3J = 9 Hz, H-8), 7.69 (2H, d, ^3J = 9 Hz, H-9), 7.76 (2H, d, ^3J = 9 Hz, H-13), 7.85 (2H, d, ^3J = 9 Hz, H-12), 8.66 (1H, s, NH). ^{13}C NMR (DMSO-d_6, 100.6 MHz, δ (ppm)): 55.4 (OCH_3-18), 55.5 (OCH_3-17), 62.2 (CH-5), 110.6 (CH-16), 111.9 (CH-19), 113.5 (CH-4), 115.9 (CH-8), 119.0 (CH-20), 121.1 (CH-12), 126.3 (CH-13), 127.0 (CH-9), 128.9 (C-15), 130.8 (C-3), 135.1 (C-10), 139.3 (C-14), 139.8 (C-11), 144.9 (C-7), 148.44 (C-18), 148.9 (C-17), 166.4 (CO-2). ^{15}N NMR (DMSO-d_6, 60.8 MHz, δ (ppm)): 88.4 (NH), 96.1 (2×NH_2), 144.1 (N). HRMS (MALDI-TOF/TOF) m/z calcd for $[M + H]^+$, 545.11200; found, 544.98933.

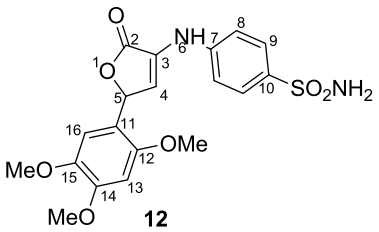

12

4-((2-Oxo-5-(2,4,5-trimethoxyphenyl)-2,5-dihydrofuran-3-yl)-amino)benzenesulfonamide ***12***. Orange solid; 71% yield; mp 169−170 °C; IR ATR ν (cm^{-1}): 3317, 3256, 2985, 2897, 2353, 1751, 1658, 1593, 1516, 1466, 1404, 1327, 1273, 1207, 1157, 1037, 810, 709, 655, 536. ^{1}H NMR (DMSO-d_6, 400.1 MHz, δ (ppm)): 3.67 (3H, s, OCH_3-15), 3.83 (3H, s, OCH_3-14), 3.84 (3H, s, OCH_3-12), 6.37 (1H, d, ^3J = 2 Hz, H-5), 6.73 (1H, s, H-16), 6.79 (1H, s, H-13), 6.89 (1H, d, ^3J = 2 Hz, H-4), 7.18 (2H, s, NH_2), 7.42 (2H, d, ^3J = 9 Hz, H-8), 7.71 (2H, d, ^3J = 9 Hz, H-9), 8.80 (1H, s, NH). ^{13}C NMR (DMSO-d_6, 100.6 MHz, δ (ppm)): 55.8 (OCH_3-14), 56.4 (OCH_3-15), 56.6 (OCH_3-12), 76.8 (CH-5), 98.6 (CH-13), 111.9 (CH-16), 114.6 (C-11), 115.8 (CH-8), 117.6 (CH-4), 127.0 (CH-9), 128.0 (C-3), 135.3 (C-10), 142.7 (C-15), 144.8 (C-7), 150.5 (C-14), 152.1 (C-12), 170.2 (CO-2). ^{15}N NMR (DMSO-d_6, 60.8 MHz, δ (ppm)): 87.7 (NH), 95.4 (NH_2). HRMS (MALDI-TOF/TOF) m/z calcd for $[M + H]^+$, 421.10248; found, 421.01298.

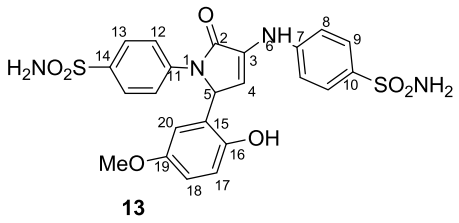

13

5-(2-Hydroxy-5-methoxyphenyl)-1-(4-sulfamoylphenyl)-3-((4-sulfamoylphenyl)amino)-1H-pyrrol-2(5H)-one ***13***. Yellow solid; 61% yield; mp 223−225 °C; IR ATR ν (cm^{-1}): 3668, 3352, 3317, 3248, 2974, 2900, 2360, 2337, 1682, 1597, 1504, 1373, 1335, 1276, 1157, 1095, 1037, 829, 760, 540. ^{1}H NMR (DMSO-d_6, 400.1 MHz, δ (ppm)): 3.54 (3H, s, CH_3-19), 6.28 (1H, d, ^3J = 3 Hz, H-5), 6.41 (1H, d, ^4J = 2 Hz, H-20), 6.55 (1H, d, ^3J = 3 Hz, H-4), 6.67 (1H, dd, ^3J = 9 Hz, ^4J = 3 Hz, H-18), 6.78 (1H, d, ^3J = 9 Hz, H-17), 7.17 (2H, s, NH_2-10), 7.26 (2H, s, NH_2-14), 7.43 (2H, d, ^3J = 9 Hz, H-8), 7.70 (2H, d, ^3J = 9 Hz, H-9), 7.77 (2H, d, ^3J = 9 Hz, H-13), 7.83 (2H, d, ^3J = 9 Hz, H-12), 8.62 (1H, s, NH), 9.52 (1H, s, OH). ^{13}C NMR (DMSO-d_6, 100.6 MHz, δ (ppm)): 55.2 (OCH_3-19), 57.4 (CH-5), 112.0 (CH-20), 112.1 (CH-4), 113.9 (CH-18), 115.8 (CH-8), 116.5 (CH-17), 120.1 (CH-12), 122.9 (C-15), 126.4 (CH-13), 127.1 (CH-9), 131.4 (C-3), 135.0 (C-10), 139.1 (C-14), 140.0 (C-11), 144.9 (C-

https://doi.org/10.1021/acs.jmedchem.3c02190
J. Med. Chem. 2024, 67, 3018−3038

7), 149.0 (C-16), 152.3 (C-19), 166.7 (CO-2). ^{15}N NMR (DMSO-d_6, 60.8 MHz, δ (ppm)): 89.2(NH), 96.4 (2×NH_2), 142.1 (N). HRMS (MALDI-TOF/TOF) m/z calcd for $[M + H]^+$, 531.09635; found, 530.97707.

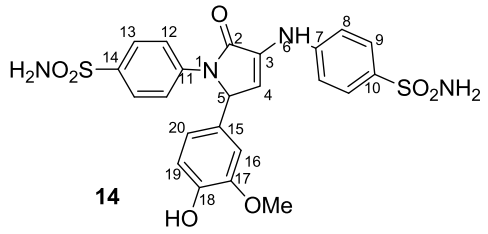

5-(4-Hydroxy-3-methoxyphenyl)-1-(4-sulfamoylphenyl)-3-((4-sulfamoylphenyl)amino)-1H-pyrrol-2(5H)-one ***14***. Brown solid; 63% yield; mp 242−243 °C; IR ATR ν (cm^{-1}): 3734, 3672, 2974, 2900, 2360, 1685, 1651, 1593, 1523, 1385, 1250, 1153, 1068, 899, 536. ^{1}H NMR (DMSO-d_6, 400.1 MHz, δ (ppm)): 3.71 (3H, s, CH_3-17), 6.06 (1H, d, ^3J = 2 Hz, H-5), 6.62 (1H, d, ^3J = 2 Hz, H-4), 6.62 (1H, d, ^4J = 2 Hz, H-16), 6.67 (2H, bs, H-19 and H-20), 6.88 (1H, bs, H-16), 7.17 (2H, s, NH_2-10), 7.25 (2H, s, NH_2-14), 7.43 (2H, d, ^3J = 9 Hz, H-8), 7.69 (2H, d, ^3J = 9 Hz, H-9), 7.78 (2H, d, ^3J = 9 Hz, H-13), 7.83 (2H, d, ^3J = 9 Hz, H-12), 8.63 (1H, s, NH), 9.01 (1H, s, OH). ^{13}C NMR (DMSO-d_6, 100.6 MHz, δ (ppm)): 55.6 (OCH_3-17), 62.3 (CH-5), 111.1 (CH-16), 113.6 (CH-4), 115.7 (CH-19), 115.9 (CH-8), 119.3 (CH-20), 121.1 (CH-12), 126.3 (CH-13), 127.3 (CH-9), 127.3 (C-15), 130.7 (C-3), 135.0 (C-10), 139.3 (C-14), 139.8 (C-11), 144.9 (C-7), 146.3 (C-18), 147.7 (C-17), 166.4 (CO-2). ^{15}N NMR (DMSO-d_6, 60.8 MHz, δ (ppm)): 88.7 (NH), 95.5 (2×NH_2), 144.1 (N). HRMS (MALDI-TOF/TOF) m/z calcd for $[M + H]^+$, 531.09635; found, 530.96502.

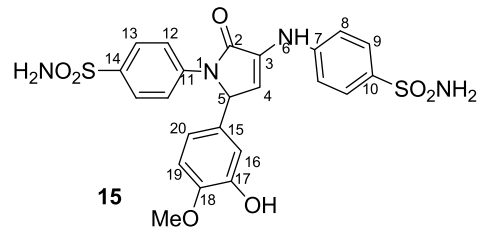

5-(3-Hydroxy-4-methoxyphenyl)-1-(4-sulfamoylphenyl)-3-((4-sulfamoylphenyl)amino)-1H-pyrrol-2(5H)-one ***15***. Yellow solid; 60% yield; mp 190−191 °C; IR ATR ν (cm^{-1}): 3672, 3313, 3252, 2974, 2900, 2360, 2337, 1685, 1651, 1593, 1543, 1504, 1385, 1335, 1269, 1149, 1076, 1045, 894, 540. ^{1}H NMR (DMSO-d_6, 400.1 MHz, δ (ppm)): 3.70 (3H, s, CH_3-18), 6.05 (1H, d, ^3J = 2 Hz, H-5), 6.61 (1H, d, ^3J = 2 Hz, H-4), 6.62 (1H, d, ^4J = 2 Hz, H-16), 6.78 (1H, dd, ^3J = 8 Hz, ^4J = 2 Hz, H-20), 6.85 (1H, d, ^3J = 8 Hz, H-19), 7.18 (2H, s, NH_2-10), 7.26 (2H, s, NH_2-14), 7.43 (2H, d, ^3J = 9 Hz, H-8), 7.70 (2H, d, ^3J = 9 Hz, H-9), 7.77 (2H, d, ^3J = 9 Hz, H-13), 7.84 (2H, d, ^3J = 9 Hz, H-12), 8.65 (1H, s, NH), 9.01 (1H, s, OH). ^{13}C NMR (DMSO-d_6, 100.6 MHz, δ (ppm)): 55.5 (OCH_3-18), 62.0 (CH-5), 112.2 (CH-19), 113.3 (CH-16), 113.7 (CH-4), 115.9 (CH-8), 118.1 (CH-20), 120.9 (CH-12), 126.4 (CH-13), 127.1 (CH-9), 129.0 (C-15), 130.6 (C-3), 135.1 (C-10), 139.3 (C-14), 139.8 (C-11), 144.9 (C-7), 146.8 (C-17), 147.5 (C-18), 166.4 (CO-2). ^{15}N NMR (DMSO-d_6, 60.8 MHz, δ (ppm)): 88.6 (NH), 96.0 (2×NH_2), 144.3 (N). HRMS (MALDI-TOF/TOF) m/z calcd for $[M + H]^+$, 531.09635; found, 531.00811.

5-(4-Hydroxy-3,5-dimethoxyphenyl)-1-(4-sulfamoylphenyl)-3-((4-sulfamoylphenyl)amino)-1H-pyrrol-2(5H)-one ***16***. Yellow solid; 59% yield; mp 233−235 °C; IR ATR ν (cm^{-1}): 3672, 3317, 3259, 2904, 2357, 2337, 1682, 1647, 1593, 1508, 1459, 1385, 1323, 1219, 1153, 1103, 1072, 1045, 813, 640, 536. ^{1}H NMR (DMSO-d_6, 400.1 MHz, δ (ppm)): 3.68 (6H, s, 2xCH_3-17), 6.06 (1H, d, ^3J = 2 Hz, H-5), 6.55 (2H, s, H-16), 6.62 (1H, d, ^3J = 2 Hz, H-4), 7.17 (2H, s, NH_2-10), 7.24 (2H, s, NH_2-14), 7.44 (2H, d, ^3J = 9 Hz, H-8), 7.69

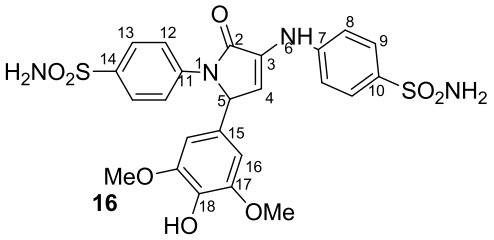

(2H, d, ^3J = 9 Hz, H-9), 7.77 (2H, d, ^3J = 9 Hz, H-13), 7.85 (2H, d, ^3J = 9 Hz, H-12), 8.38, (1H, s, OH), 8.64 (1H, s, NH). ^{13}C NMR (DMSO-d_6, 100.6 MHz, δ (ppm)): 56.0 (OCH_3-17), 62.7 (CH-5), 104.3 (CH-16), 113.5 (CH-4), 115.8 (CH-8), 121.2 (CH-12), 126.3 (CH-13), 126.6 (C-15), 127.0 (CH-9), 130.7 (C-3), 135.0 (C-10), 135.2 (C-18), 139.4 (C-14), 139.8 (C-11), 144.9 (C-7), 148.1 (C-17), 166.4 (CO-2). ^{15}N NMR (DMSO-d_6, 40.5 MHz, δ (ppm)): 88.8 (NH), 96.4 (2×NH_2), 143.8 (N). HRMS (MALDI-TOF/TOF) m/z calcd for $[M + H]^+$, 561.10691; found, 561.0142.

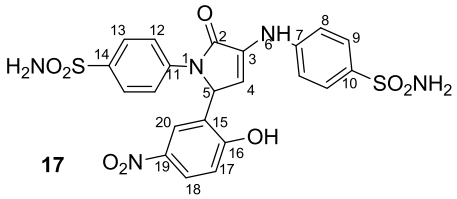

5-(2-Hydroxy-5-nitrophenyl)-1-(4-sulfamoylphenyl)-3-((4-sulfamoylphenyl)amino)-1H-pyrrol-2(5H)-one ***17***. Yellow solid; 73% yield; mp 247−248 °C; IR ATR ν (cm^{-1}): 3433, 3329, 3257, 3120, 2901, 2360, 1685, 1658, 1595, 1527, 1490, 1373, 1323, 1286, 1143, 1093, 1072, 825, 738, 653, 536. ^{1}H NMR (DMSO-d_6, 400.1 MHz, δ (ppm)): 6.39 (1H, d, ^3J = 3 Hz, H-5), 6.61 (1H, d, ^3J = 3 Hz, H-4), 6.99 (1H, d, ^3J = 9 Hz, H-17), 7.17 (2H, s, NH_2-10), 7.26 (2H, s, NH_2-14), 7.44 (2H, d, ^3J = 9 Hz, H-8), 7.69 (2H, d, ^3J = 9 Hz, H-9), 7.78 (2H, d, ^3J = 9 Hz, H-13), 7.83 (2H, d, ^3J = 9 Hz, H-12), 7.94 (1H, bs, H-20), 8.02 (1H, dd, ^3J = 9 Hz, ^4J = 3 Hz, H-18), 8.71 (1H, s, NH), 11.63 (1H, s, OH). ^{13}C NMR (DMSO-d_6, 100.6 MHz, δ (ppm)): 58.0 (CH-5), 110.53 (CH-4), 115.9 (CH-8), 116.3 (CH-17), 120.3 (CH-12), 123.7 (CH-20 and C-15), 125.4 (CH-18), 126.5 (CH-13), 127.0 (CH-9), 132.0 (C-3), 135.2 (C-10), 139.4 (C-14), 139.6 (C-19), 139.7 (C-11), 144.7 (C-7), 161.8 (C-16), 166.6 (CO-2). HRMS (MALDI-TOF/TOF) m/z calcd for $[M + H]^+$, 546.07086; found, 545.94410.

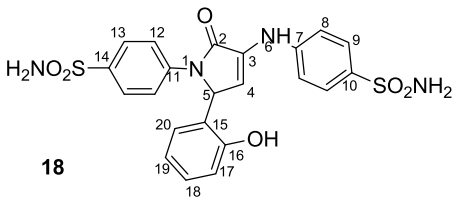

5-(2-Hydroxyphenyl)-1-(4-sulfamoylphenyl)-3-((4-sulfamoylphenyl)amino)-1H-pyrrol-2(5H)-one ***18***. Yellow solid; 57% yield; mp 265−267 °C; IR ATR ν (cm^{-1}): 3672, 3317, 3255, 2974, 2901, 2360, 1681, 1597, 1539, 1392, 1327, 1253, 1149, 1064, 895, 825, 540. ^{1}H NMR (DMSO-d_6, 400.1 MHz, δ (ppm)): 6.33 (1H, d, ^3J = 3 Hz, H-5), 6.58 (1H, d, ^3J = 3 Hz, H-4), 6.69 (1H, t, ^3J = 7 Hz, H-19), 6.84−6.88 (2H, m, H-17 and H-20), 7.06 (1H, t, ^3J = 7 Hz, H-18), 7.18 (2H, s, NH_2-10), 7.27 (2H, s, NH_2-14), 7.43 (2H, d, ^3J = 9 Hz, H-8), 7.70 (2H, d, ^3J = 9 Hz, H-9), 7.77 (2H, d, ^3J = 9 Hz, H-13), 7.84 (2H, d, ^3J = 9 Hz, H-12), 8.63 (1H, s, NH), 10.02 (1H, s, OH). ^{13}C NMR (DMSO-d_6, 100.6 MHz, δ (ppm)): 57.2 (CH-5), 112.3 (CH-4), 115.8 (CH-17) 115.9 (CH-8), 119.6 (CH-19), 120.0 (CH-12), 122.1(C-15), 126.4 (CH-13), 126.8 (CH-20), 127.1 (CH-9), 128.9 (CH-18), 131.3 (C-3), 135.1 (C-10), 139.0 (C-14), 140.1 (C-11), 144.9 (C-7), 155.2 (C-16), 166.8 (C-2). ^{15}N NMR (DMSO-d_6, 40.5 MHz, δ (ppm)): 89.3 (NH), 96.1 (2×NH_2), 142.6 (N).

https://doi.org/10.1021/acs.jmedchem.3c02190
J. Med. Chem. 2024, 67, 3018−3038

HRMS (MALDI-TOF/TOF) m/z calcd for $[M + H]^+$, 501.08578; found, 500.96602.

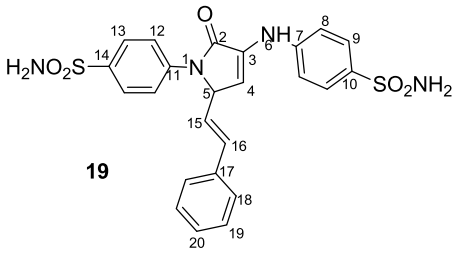

4-((2-Oxo-5-styryl-1-(4-sulfamoylphenyl)-2,5-dihydro-1H-pyrrol-3-yl)amino)benzenesulfonamide ***19***. Yellow solid; 49% yield; mp 218−220 °C; IR ATR ν (cm^{-1}): 3672, 3325, 3236, 2974, 2900, 2017, 1975, 1686, 1651, 1589, 1539, 1493, 1373, 1319, 1253, 1149, 1068, 1053, 902, 829, 686, 540. ^{1}H NMR (DMSO-d_6, 600.1 MHz, δ (ppm)): 5.74 (1H, dd, ^3J = 8 Hz, 2 Hz, H-5), 5.95 (1H, dd, ^3J = 16 Hz, 8 Hz, H-15), 6.58 (1H, d, ^3J = 2 Hz, H-4), 6.96 (1H, d, ^3J = 16 Hz, H-16), 7.19 (2H, s, NH_2-10), 7.24 (1H, t, ^3J = 7 Hz, H-20), 7.27 (2H, s, NH_2-14), 7.30 (2H, t, ^3J = 7 Hz, H-19), 7.41 (2H, d, ^3J = 7 Hz, H-18), 7.48 (2H, d, ^3J = 9 Hz, H-8), 7.72 (2H, d, ^3J = 9 Hz, H-9), 7.85 (2H, d, ^3J = 9 Hz, H-13), 7.93 (2H, d, ^3J = 9 Hz, H-12), 8.69 (1H, s, NH). ^{13}C NMR (DMSO-d_6, 150.9 MHz, δ (ppm)): 61.4 (CH-5), 110.5 (CH-4), 116.0 (CH-8), 121.0 (CH-12), 126.1 (CH-15), 126.4 (CH-13), 126.5 (CH-18), 127.0 (CH-9), 128.0 (CH-20), 128.6 (CH-19), 132.1 (C-3), 134.1 (CH-16), 135.2 (C-10), 135.7 (CH-17), 139.4 (C-14), 139.9 (C-11), 144.8 (C-7), 165.9 (CO-2). ^{15}N NMR (DMSO-d_6, 60.8 MHz, δ (ppm)): 89.2 (NH), 95.7 (2×NH_2), 141.1 (N). HRMS (MALDI-TOF/TOF) m/z calcd for $[M + H]^+$, 511.10652; found, 511.00329.

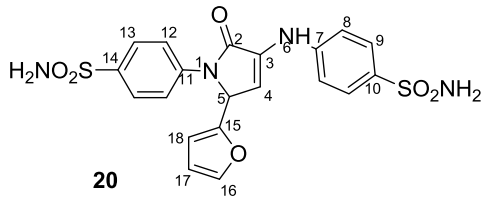

5-(Furan-2-yl)-1-(4-sulfamoylphenyl)-3-((4-sulfamoylphenyl)-amino)-1H-pyrrol-2(5H)-one ***20***. Red solid; 83% yield; mp 255−257 °C; IR ATR ν (cm^{-1}): 3672, 3325, 3251, 2986, 2900, 2360, 1693, 1658, 1593, 1539, 1500, 1369, 1339, 1319, 1149, 1068, 1053, 906, 829, 651, 540. ^{1}H NMR (DMSO-d_6, 400.1 MHz, δ (ppm)): 6.37−6.38 (2H, m, H-5 and H-17), 6.60 (1H, d, ^3J = 3 Hz, H-18), 6.65 (1H, d, ^3J = 2 Hz, H-4), 7.20 (2H, s, NH_2-10), 7.32 (2H, s, NH_2-14), 7.48 (2H, d, ^3J = 9 Hz, H-8), 7.54 (1H, bs, H-16), 7.73 (2H, d, ^3J = 9 Hz, H-9), 7.82 (2H, d, ^3J = 9 Hz, H-13), 7.87 (2H, d, ^3J = 9 Hz, H-12), 8.73 (1H, s, NH). ^{13}C NMR (DMSO-d_6, 100.6 MHz, δ (ppm)): 56.4 (CH-5), 109.1 (CH-5), 110.1 (CH-18), 110.6 (CH-17), 116.1 (CH-8), 121.1 (CH-12), 126.4 (CH-13), 127.1 (CH-9), 132.0 (C-3), 135.2 (C-10), 139.4 (C-14), 139.7 (C-11), 143.4 (CH-16), 144.7 (C-7), 148.6 (C-15), 165.9 (CO-2). ^{15}N NMR (DMSO-d_6, 60.8 MHz, δ (ppm)): 89.5 (NH), 95.9 (2×NH_2), 139.9 (N). HRMS (MALDI-TOF/TOF) m/z calcd for $[M + H]^+$, 475.07013; found, 474.99819.

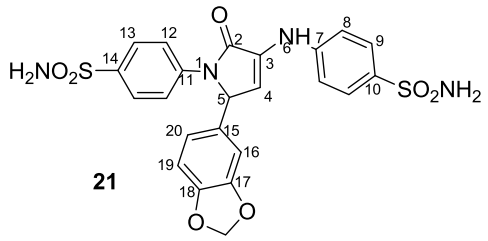

5-(Benzo[d][1,3]dioxol-5-yl)-1-(4-sulfamoylphenyl)-3-((4-sulfamoylphenyl)amino)-1H-pyrrol-2(5H)-one ***21***. Yellow solid; 80% yield; mp 232−233 °C; IR ATR ν (cm^{-1}): 3672, 3302, 2981, 2900, 2357, 2333, 1693, 1651, 1597, 1539, 1504, 1392, 1334, 1249, 1149, 1041, 825, 651, 540. ^{1}H NMR (DMSO-d_6, 400.1 MHz, δ (ppm)): 5.95−5.96 (2H, m, CH_2), 6.11 (1H, d, ^3J = 2 Hz, H-5), 6.60 (1H, d, ^3J = 2 Hz, H-4), 6.81 (1H, bs, H-16), 6.85 (2H, bs, H-19 and H-20), 7.17 (2H, s, NH_2-10), 7.28 (2H, s, NH_2-14), 7.44 (2H, d, ^3J = 9 Hz, H-8), 7.69 (2H, d, ^3J = 9 Hz, H-9), 7.78 (2H, d, ^3J = 9 Hz, H-13), 7.83 (2H, d, ^3J = 9 Hz, H-12), 8.66 (1H, s, NH). ^{13}C NMR (DMSO-d_6, 100.6 MHz, δ (ppm)): 62.0 (CH-5), 101.1 (CH_2), 106.8 (CH-16), 108.4 (CH-19), 113.1 (CH-4), 115.9 (CH-8), 120.7 (CH-20), 121.1 (CH-12), 126.3 (CH-13), 127.1 (CH-9), 130.6 (C-15), 130.9 (C-3), 135.1 (C-10), 139.4 (C-14), 139.6 (C-11), 144.8 (C-7), 147.0 (C-18), 147.6 (C-17), 166.3 (CO-2). ^{15}N NMR (DMSO-d_6, 60.8 MHz, δ (ppm)): 88.6 (NH), 96.2 (2×NH_2), 144.1 (N). HRMS (MALDI-TOF/TOF) m/z calcd for $[M + H]^+$, 529.08070; found, 528.97968.

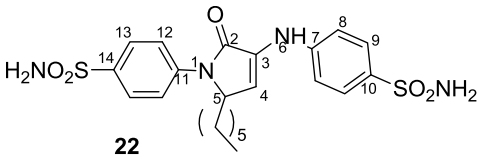

5-Hexyl-1-(4-sulfamoylphenyl)-3-((4-sulfamoylphenyl)amino)-1H-pyrrol-2(5H)-one ***22***. Yellow solid; 49% yield; mp 255−256 °C; IR ATR ν (cm^{-1}): 3672, 3387, 3275, 2970, 2900, 2360, 2333, 1685, 1654, 1597, 1543, 1505, 1396, 1338, 1311, 1153, 1064, 898, 825, 682, 655, 543. ^{1}H NMR (DMSO-d_6, 400.1 MHz, δ (ppm)): 0.78 (3H, t, ^3J = 7 Hz, CH_3), 0.85−0.90, 1.09−1.50, 1.77−1.83 (10H, m, 5×CH_2), 5.10−5.13 (1H, m, H-5), 6.68 (1H, d, ^3J = 2 Hz, H-4), 7.18 (2H, s, NH_2-10), 7.36 (2H, s, NH_2-14), 7.44 (2H, d, ^3J = 9 Hz, H-8), 7.72 (2H, d, ^3J = 9 Hz, H-9), 7.83 (2H, d, ^3J = 9 Hz, H-13), 7.90 (2H, d, ^3J = 9 Hz, H-12), 8.53 (1H, s, NH). ^{13}C NMR (DMSO-d_6, 150.9 MHz, δ (ppm)): 13.7 (CH_3), 21.8, 22.3, 30.5, 31.0 (5×CH_2), 58.4 (CH-5), 112.1 (CH-4), 115.8 (CH-8), 121.6 (CH-12), 126.6 (CH-13), 127.1 (CH-9), 131.2 (C-3), 134.9 (C-10), 139.4 (C-14), 139.7 (C-11), 145.1 (C-7), 165.7 (CO-2). ^{15}N NMR (DMSO-d_6, 40.5 MHz, δ (ppm)): 89.3 (NH), 95.5 (2×NH_2), 142.4 (N). HRMS (MALDI-TOF/TOF) m/z calcd for $[M + H]^+$, 493.15347; found, 493.02991.

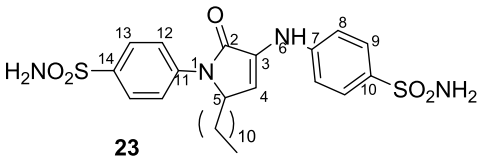

5-Undecyl-1-(4-sulfamoylphenyl)-3-((4-sulfamoylphenyl)-amino)-1H-pyrrol-2(5H)-one ***23***. Yellow solid; 47% yield; mp 260−262 °C; IR ATR ν (cm^{-1}): 3672, 3317, 3255, 2974, 2901, 2360, 1681, 1597, 1539, 1392, 1327, 1253, 1149, 1064, 895, 825, 540. ^{1}H NMR (DMSO-d_6, 600.1 MHz, δ (ppm)): 0.85 (3H, t, ^3J = 7 Hz, CH_3), 1.16−1.27 (18H, m, 9× CH_2), 1.46−1.48 and 1.77−1.82 (2H, m, CH_2), 5.10−5.12 (1H, m, H-5), 6.68 (1H, d, ^3J = 2 Hz, H-4), 7.18 (2H, s, NH_2-10), 7.36 (2H, s, NH_2-14), 7.44 (2H, d, ^3J = 9 Hz, H-8), 7.71 (2H, d, ^3J = 9 Hz, H-9), 7.83 (2H, d, ^3J = 9 Hz, H-13), 7.89 (2H, d, ^3J = 9 Hz, H-12), 8.54 (1H, s, NH). ^{13}C NMR (DMSO-d_6, 150.9 MHz, δ (ppm)): 13.9 (CH_3), 22.0, 22.7, 28.6, 28.8, 29,0, 30.6, 31.2 (10×CH_2), 58.4 (CH-5), 112.1 (CH-4), 115.7 (CH-8), 121.5 (CH-12), 126.6 (CH-13), 127.0 (CH-9), 131.9 (C-3), 134.9 (C-10), 139.4 (C-14), 139.7 (C-11), 145.0 (C-7), 165.7 (CO-2). ^{15}N NMR (DMSO-d_6, 60.8 MHz, δ (ppm)): 89.0 (NH), 95.6 (2×NH_2), 141.3 (N). HRMS (MALDI-TOF/TOF) m/z calcd for $[M + H]^+$, 563.23172; found, 563.09800.

Computational Method. DFT calculations were used to perform geometry optimization of the neutral form of the general imine structure A (Scheme 3) using the B3LYP functional and 6-311++G(d,p) basis set for all atoms. These calculations were done using the Gaussian 16[57] software package. To predict reactive sites in an electrophilic reaction, the Fukui function f^- is known to be very useful

https://doi.org/10.1021/acs.jmedchem.3c02190
J. Med. Chem. 2024, 67, 3018−3038

and is widely employed, and some of us have successfully applied it to a variety of systems in previous investigations.[58−60] The use of the DFT approach for the calculation of the Fukui function was first introduced by Parr and Yang.[48] The Fukui function f^- is defined as

$$f^-(\vec{r}) = \rho_N(\vec{r}) - \rho_{N+1}(\vec{r})$$

with $\rho_N(\vec{r})$ being the electronic density of the optimized neutral form and $\rho_{N+1}(\vec{r})$ of the corresponding cationic form with the same geometry. We also calculated the condensed cf function in which instead of the electronic density are used the atomic charges, using the ADCH (atomic dipole moment corrected Hirshfeld population) charges.[61] All if these properties were calculated with Multiwfn.[62] Molecular model representations were generated using VMD software.[63]

Carbonic Anhydrase Inhibition. An Applied Photophysics stopped-flow instrument was used to assay the CA-catalyzed CO_2 hydration activity.[49] Phenol red (at a concentration of 0.2 mM) was used as an indicator, working at an absorbance maximum of 557 nm, with 20 mM Hepes (pH 7.4) as a buffer and 20 mM Na_2SO_4 (to maintain constant ionic strength), following the initial rates of the CA-catalyzed CO_2 hydration reaction for a period of 10−100 s. The CO_2 concentrations ranged from 1.7 to 17 mM for the determination of the kinetic parameters and inhibition constants.[64] Enzyme concentrations ranged between 5 and 12 nM. For each inhibitor, at least six traces of the initial 5−10% of the reaction were used to determine the initial velocity. The uncatalyzed rates were determined in the same manner and subtracted from the total observed rates. Stock solutions of the inhibitor (0.1 mM) were prepared in distilled-deionized water and dilutions up to 0.01 nM were done thereafter with the assay buffer. Inhibitor and enzyme solutions were preincubated together for 15 min at room temperature prior to the assay, to allow for the formation of the E−I complex. The inhibition constants were obtained by nonlinear least-squares methods using PRISM 3 and the Cheng−Prusoff equation as reported earlier and represent the mean from at least three different determinations. All CA isoforms were recombinant proteins obtained in house, as reported earlier.[65−67]

Molecular Modeling. The crystal structures of CA I (PDB: 2NMX),[51] CA II (PDB: 3K34),[52] CA IX (PDB: 5FL4),[53] and CA XII (PDB: 1JD0)[54] used for computational studies were downloaded by Protein Data Bank[68] and prepared according to the Protein Preparation module in Maestro Schrödinger suite, assigning bond orders, adding hydrogens, deleting water molecules, and optimizing H-bonding networks. Finally, energy minimization with a root means square deviation (RMSD) value of 0.30 was applied using an optimized potential for liquid simulation (OPLS4) force field.[69−77] Grids for docking were centered in the centroid of the complexed ligand. Docking studies were carried out with the program Glide[73] using the standard precision (SP) mode. 3D ligand structures were prepared by Maestro.[74] Figures were generated with Maestro and Chimera.[78]

Crystallization and X-ray Data Collection. Crystals of hCA II were obtained using the hanging drop vapor diffusion method using a 24-well Linbro plate. 2 μL of 10 mg/mL solution of hCA II in Tris-HCl, 20 mM, pH 8.0, were mixed with 2 μL of a solution of 1.5 M sodium citrate, 0.1 M Tris pH 8.0 and were equilibrated against the same solution at 296 K. The complexes were prepared by soaking the hCA II native crystals in the mother liquor solution containing the inhibitors at a concentration of 10 mM for 2 days. All crystals were flash-frozen at 100 K using a solution obtained by adding 15% (v/v) glycerol to the mother liquor solution as cryoprotectant. Data on crystals of the complexes were collected using synchrotron radiation at the XRD2 beamline at Elettra Synchrotron (Trieste, Italy) with a wavelength of 1.000 Å and a DECTRIS Pilatus 6 M detector. Data were integrated and scaled using the program energy-dispersive X-ray spectrum (XDS).[79] Data processing statistics are shown in the Supporting Information.

Structure Determination. The crystal structure of hCA II (PDB accession code: 4FIK) without solvent molecules and other heteroatoms was used to obtain initial phases using Refmac5.[80] 5% of the unique reflections were selected randomly and excluded from the refinement data set for the purpose of Rfree calculations. The initial $|F_o - F_c|$ difference electron density maps unambiguously showed the inhibitor molecules. The inhibitor was introduced in the model with 1.0 occupancy. Refinements proceeded using normal protocols of positional, isotropic atomic displacement parameters alternating with manual building of the models using COOT.[81] The quality of the final models was assessed with COOT and RAMPAGE.[82] Crystal parameters and refinement data are summarized in the Supporting Information. Atomic coordinates were deposited in the Protein Data Bank (PDB accession code: 8R2K). Graphical representations were generated with Chimera.[78]

Cell Culture. MCF7 human breast adenocarcinoma cell line was purchased from ATCC (ATCC HTB-22TM) (Rockville, MD) and cultured in Dulbecco's modified Eagle's medium (DMEM) high glucose with 10% fetal bovine serum (FBS), 1% penicillin/streptomycin, and 1% L-glutamine (all purchased from Euro-Clone, Milan, Italy). Cell culture was kept at 37 °C in a humidified atmosphere with 5% CO_2. Cells at passages 10−20 were used for the experimental evaluations.

***In Vitro* Hypoxia Induction and Cell Treatment.** MCF7 were seeded in a tissue culture-treated 96-well plate at a density of 10,000/well and let adhere for 24 h. After 24 h, a fresh medium containing $CoCl_2$ 100 μM was added to induce hypoxia, as reported elsewhere.[56] $CoCl_2$ was maintained within the culture medium for 48 h, renewing the medium every 24 h. After that, the treatment with doxo alone at 2.5 μM and in combination with newly synthesized compounds, namely, **9**, **14**, **16**, and **20**, at 50 μM, previously dissolved in DMSO, was started and kept up to 72 h. The final concentration of DMSO was established at 0.1% in all experimental points. Inner controls, represented by cells exposed to $CoCl_2$ alone, DMSO alone, and DMSO+$CoCl_2$ were also added to the experimental panel.

Metabolic Activity Assay (MTT). To establish MCF7 metabolic activity, an 3-(4,5-dimethylthiazol-2-yl)-2,5-diphenyltetrazolium bromide (MTT) (Merck, Milan, Italy) test, after 72 h of treatment in the presence of doxo 2.5 μM alone and in combination with compounds **9**, **14**, **16**, and **20** at 50 μM, under hypoxic conditions, was carried out. Culture medium was added with 10% MTT and incubated for 4 h at 37 °C. Medium containing MTT was discarded and replaced by an equal volume of DMSO to dissolve formazan crystals. The final solution was spectrophotometrically read by a microplate reader (Multiskan GO, Thermo Scientific, Waltham, MA) at 540 nm. The sample represented by cells exposed to DMSO+$CoCl_2$ was assumed as the control; metabolic activity values were normalized to the control and expressed as percentage. The assay was performed in triplicate.

Lactate Dehydrogenase (LDH) Assay. In order to establish the cytotoxicity level provoked by doxo 2.5 μM alone and in combination with compounds **9**, **14**, **16**, and **20** at 50 μM on MCF7, under hypoxic conditions, a LDH assay, quantifying the amount of released LDH within the culture medium, was performed, after 72 h of treatment, by CytoTox 96 nonradioactive cytotoxicity assay (Promega, Madison, WI), following the manufacturer's instructions. The measured LDH release was normalized with MTT optical density (OD) values. The assay was performed in triplicate.

Statistical Analysis. Statistical analysis was carried out with GraphPad 8 software by ordinary one-way analysis of variance (ANOVA), followed by Dunnett's *post hoc* multiple comparisons test. DMSO+$CoCl_2$ was chosen as the control sample.

■ ASSOCIATED CONTENT

Supporting Information

The Supporting Information is available free of charge at https://pubs.acs.org/doi/10.1021/acs.jmedchem.3c02190.

Molecular formula strings (CSV)

CAI_9R (PDB)

CAI_9S (PDB)

https://doi.org/10.1021/acs.jmedchem.3c02190
J. Med. Chem. 2024, 67, 3018−3038

CAI_12R (PDB)
CAI_12S (PDB)
CAII_9R (PDB)
CAII_9S (PDB)
CAII_12R (PDB)
CAII_12S (PDB)
CAIX_9R (PDB)
CAIX_9S (PDB)
CAIX_12R (PDB)
CAIX_12S (PDB)
CAXII_9R (PDB)
CAXII_9S (PDB)
CAXII_12R (PDB)
CAXII_12S (PDB)

^{1}H NMR, ^{13}C NMR, MALDI-MS, and FT-IR spectra of compound **1** (Figure S1); ^{1}H NMR, ^{13}C NMR, ^{19}F NMR, MALDI-MS, and FT-IR spectra of compound **2** (Figure S2); ^{1}H NMR, ^{13}C NMR, ^{19}F NMR, ^{1}H,^{13}C HMBC, MALDI-MS, and FT-IR spectra of compound **5** (Figure S3); ^{1}H NMR, ^{13}C NMR, MALDI-MS, and FT-IR spectra of compound **11** (Figure S4); ^{1}H NMR, ^{13}C NMR, MALDI-MS, and FT-IR spectra of compound **19** (Figure S5); ^{1}H NMR, ^{13}C NMR, MALDI-MS, and FT-IR spectra of compound **20** (Figure S6); ^{1}H NMR, ^{13}C NMR, MALDI-MS, and FT-IR spectra of compound **23** (Figure S7); ^{1}H NMR, ^{13}C NMR, MALDI-MS, and FT-IR spectra of compound **12** (Figure S8); atom numbering of compound A (Figure S9); condensed Fukui function f^{-} for the atoms in compound A (Table SI.1); summary of data collection and atomic model refinement statistics for hCA II (Table SI.2); electron density of inhibitor **12** bound to zinc (gray) in hCA II active site; $2F_o-F_c$ maps contoured to the 1.0 σ level (Figure S10); PDB ID for carbonic anhydrase isoforms (CA) (Table SI.3); HPLC spectra for compound **14** (280 nm) (Figure S11); HPLC spectra for compound **9** (280 nm) (Figure S12); and HPLC spectra for compound **20** (280 nm) (Figure S13) (PDF)

AUTHOR INFORMATION

Corresponding Authors

Cristina M. Al-Matarneh − *Center of Advanced Research in Bionanoconjugates and Biopolymers, "Petru Poni" Institute of Macromolecular Chemistry of Romanian Academy, Iasi 700487, Romania; Research Institute of the University of Bucharest-ICUB, 050663 Bucharest, Romania;* orcid.org/0000-0001-9299-1347; Email: almatarneh.cristina@icmpp.ro

Mariana Pinteala − *Center of Advanced Research in Bionanoconjugates and Biopolymers, "Petru Poni" Institute of Macromolecular Chemistry of Romanian Academy, Iasi 700487, Romania*; Email: pinteala@icmpp.ro

Andrea Angeli − *Sezione di Scienze Farmaceutiche, NeuroFarba Department, Universita degli Studi di Firenze, 50019 Sesto Fiorentino, Italy;* orcid.org/0000-0002-1470-7192; Email: andrea.angeli@unifi.it

Authors

Alina Nicolescu − *NMR Laboratory "Petru Poni" Institute of Macromolecular Chemistry of Romanian Academy, Iasi 700487, Romania*

Mihaela Silion − *Physics of Polymers and Polymeric Materials Department, "Petru Poni" Institute of Macromolecular Chemistry, 700487 Iasi, Romania*

Francesca Mocci − *Department of Chemical and Geological Sciences, University of Cagliari, 09124 Cagliari, Italy;* orcid.org/0000-0003-1394-9146

Razvan Puf − *Center of Advanced Research in Bionanoconjugates and Biopolymers, "Petru Poni" Institute of Macromolecular Chemistry of Romanian Academy, Iasi 700487, Romania*

Marta Ferraroni − *Dipartimento di Chimica "Ugo Schiff", University of Florence, 50019 Sesto Fiorentino, Florence, Italy;* orcid.org/0000-0001-7258-738X

Claudiu T. Supuran − *Sezione di Scienze Farmaceutiche, NeuroFarba Department, Universita degli Studi di Firenze, 50019 Sesto Fiorentino, Italy;* orcid.org/0000-0003-4262-0323

Susi Zara − *Department of Pharmacy, "G. d'Annunzio" University of Chieti-Pescara, 66100 Chieti, Italy*

Simone Carradori − *Department of Pharmacy, "G. d'Annunzio" University of Chieti-Pescara, 66100 Chieti, Italy;* orcid.org/0000-0002-8698-9440

Niccolò Paoletti − *Department of Chemical and Geological Sciences, University of Cagliari, 09124 Cagliari, Italy; Sezione di Scienze Farmaceutiche, NeuroFarba Department, Universita degli Studi di Firenze, 50019 Sesto Fiorentino, Italy;* orcid.org/0000-0002-6874-9419

Alessandro Bonardi − *Sezione di Scienze Farmaceutiche, NeuroFarba Department, Universita degli Studi di Firenze, 50019 Sesto Fiorentino, Italy; NEUROFARBA Department, Pharmaceutical and Nutraceutical Section, Laboratory of Molecular Modeling Cheminformatics & QSAR, University of Florence, 50019 Sesto Fiorentino, Firenze, Italy*

Paola Gratteri − *NEUROFARBA Department, Pharmaceutical and Nutraceutical Section, Laboratory of Molecular Modeling Cheminformatics & QSAR, University of Florence, 50019 Sesto Fiorentino, Firenze, Italy;* orcid.org/0000-0002-9137-2509

Complete contact information is available at: https://pubs.acs.org/10.1021/acs.jmedchem.3c02190

Author Contributions

The manuscript was written through contributions of all authors. All authors have given approval to the final version of the manuscript. Synthesis was conducted by C.M.A.-M.; phisicochemical characterization was made by C.M.A.-M., A.N., and M.S.; computational methods were realized by F.M. and R.P.; X-ray studies were conducted by M.F.; carbonic anhydrase inhibition experiments were conducted by A.A., S.C., and C.T.S.; molecular modeling was realized by N.P., A.B., and P.G.; cell-based biological assays were conducted by S.Z.; conceptualization was made by M.P. and C.M.A.-M. The authors will release the atomic coordinates upon article publication.

Funding

This paper is supported by the European Union's Horizon Europe research and innovation program under Grant Agreement No. 101086667, Project BioMat4CAST (BioMat4CAST—"Petru Poni" Institute of Macromolecular Chemistry Multi-Scale In Silico Laboratory for Complex and Smart Biomaterials).

Notes

The authors declare no competing financial interest.

■ ACKNOWLEDGMENTS

C.M.A.-M. acknowledge the support provided by the ICUB Fellowship for Young Researchers (A.C.M., Contract No. 26260/5.12.2022). The authors also acknowledge the support provided by European Union's Horizon Europe research and innovation programme under Grant Agreement No. 101086667, Project BioMat4CAST (BioMat4CAST—"Petru Poni" Institute of Macromolecular Chemistry Multi-Scale In Silico Laboratory for Complex and Smart Biomaterials). The authors gratefully acknowledge Elettra and XRD2 beamline for providing beamtime and support under Proposal 20220596.

■ ABBREVIATIONS USED

CA carbonic anhydrase
DPO dihydro-pyrrol-2-one
hCA human carbonic anhydrase

■ REFERENCES

(1) Lashkari, M.; Maghsoodlou, M. T.; Karima, M.; Kangani, M. Trifluoroacetic Acid Catalyzed One-Pot Four-Component Domino Reaction for the Synthesis of Substituted Dihydro 2-Oxypyrroles. *J. Chil. Chem. Soc.* **2018**, *1*, 3799−3802.

(2) Cusumano, A. Q.; Pierce, J. G. 3-Hydroxy-1,5-Dihydro-2H-Pyrrol-2-Ones as Novel Antibacterial Scaffolds against Methicillin-Resistant Staphylococcus Aureus. *Bioorg. Med. Chem. Lett.* **2018**, *28* (16), 2732−2735.

(3) Li, Y.; Ouyang, Y.; Wu, H.; Wang, P.; Huang, Y.; Li, X.; Chen, H.; Sun, Y.; Hu, X.; Wang, X.; Li, G.; Lu, Y.; Li, C.; Lu, X.; Pang, J.; Nie, T.; Sang, X.; Dong, L.; Dong, W.; Jiang, J.; Paterson, I. C.; Yang, X.; Hong, W.; Wang, H.; You, X. The Discovery of 1, 3-Diamino-7H-Pyrrol[3, 2-f]Quinazoline Compounds as Potent Antimicrobial Antifolates. *Eur. J. Med. Chem.* **2022**, *228*, 113979−113996.

(4) Gao, Y.; Samanta, S.; Cui, T.; Lam, Y. Synthesis and in Vitro Evaluation of West Nile Virus Protease Inhibitors Based on the 1,3,4,5-Tetrasubstituted 1H-Pyrrol-2(5H)-One Scaffold. *ChemMedChem* **2013**, *8* (9), 1554−1560.

(5) Demirayak, S.; Çagri, A.; Kiraz, N. Synthesis and Antibacterial Activities of Some 1-[2-(Substituted Pyrrol-1-Yl)Ethyl]-2-Methyl-5-Nitroimidazole Derivatives. *Eur. J. Med. Chem.* **1999**, *34*, 275−278.

(6) Kirpotina, L. N.; Schepetkin, I. A.; Khlebnikov, A. I.; Ruban, O. I.; Ge, Y.; Ye, R. D.; Kominsky, D. J.; Quinn, M. T. 4-Aroyl-3-Hydroxy-5-Phenyl-1 H -Pyrrol-2 (5 H) -Ones as N -Formyl Peptide Receptor 1 (FPR1) Antagonists. *Biochem. Pharmacol.* **2017**, *142*, 120−132.

(7) Geng, Y.; Wang, X.; Yang, L.; Sun, H.; Wang, Y.; Zhao, Y.; et al. Antitumor Activity of a 5-Hydroxy-1 H -Pyrrol- 2- (5 H) -One-Based Synthetic Small Molecule In Vitro and In Vivo. *PLoS One* **2015**, *10* (6), No. e0128928.

(8) El-Desouky, S. K.; Kim, K. H.; Ryu, S. Y.; Eweas, A. F.; Gamal-Eldeen, A. M.; Kim, Y. A New Pyrrole Alkaloid Isolated from Arum Palaestinum Boiss. and Its Biological Activities. *Arch Pharm. Res.* **2007**, *30* (8), 927−931.

(9) Alizadeh, N.; Hossein Sayahi, M.; Iraji, A.; Yazzaf, R.; Moazzam, A.; Mobaraki, K.; Adib, M.; Attarroshan, M.; Larijani, B.; Rastegar, H.; Khoshneviszadeh, M.; Mahdavi, M. Evaluating the Effects of Disubstituted 3-Hydroxy-1H-Pyrrol-2(5H)-One Analog as Novel Tyrosinase Inhibitors. *Bioorg. Chem.* **2022**, *126*, 105876−105885.

(10) Alp, C.; Ekinci, D.; Serdar, M.; Murat, S.; et al. A Novel and One-Pot Synthesis of New 1-Tosyl Pyrrol-2-One Derivatives and Analysis of Carbonic Anhydrase Inhibitory Potencies. *Bioorg. Med. Chem.* **2010**, *18*, 4468−4474.

(11) Reddy, T. R. K.; Li, C.; Guo, X.; Myrvang, H. K.; Fischer, P. M.; Dekker, L. V. Design, Synthesis, and Structure−Activity Relationship Exploration of 1-Substituted 4-Aroyl-3-Hydroxy-5-Phenyl-1 H -Pyrrol-2(5 H)-One Analogues as Inhibitors of the Annexin A2−S100A10 Protein Interaction. *J. Med. Chem.* **2011**, *54* (7), 2080−2094.

(12) Peifer, C.; Selig, R.; Kinkel, K.; Ott, D.; Totzke, F.; Schächtele, C.; Heidenreich, R.; Röcken, M.; Schollmeyer, D.; Laufer, S. Design, Synthesis, and Biological Evaluation of Novel 3-Aryl-4- (1 H -Indole-3yl) −1, 5-Dihydro-2 H -Pyrrole-2-Ones as Vascular Endothelial Growth Factor Receptor (VEGF-R) Inhibitors. *J. Med. Chem.* **2008**, *51* (13), 3814−3824.

(13) Rad-Moghadam, K.; Esmaeili, A. A.; Ghalandarabad, S. A.; Hoseininejad, F.; Fallah-Rasoulinejad, S. A.; Kiani, S. Synthesis of Novel 1-(Benzo[d]Thiazol-2-yl)-1 H -pyrrol-2(5 H)-ones. *J. Heterocycl. Chem.* **2014**, *51* (6), 1791−1796.

(14) Tatibouët, A.; Fixler, N.; Demeunynck, M.; Lhomme, J. Reaction of 3-Amino-Acridine with Formaldehyde in Acidic Medium: Influence of the Stoechiometry on the Reaction Products. *Tetrahedron* **1997**, *53* (8), 2891−2898.

(15) Zali-boeini, H.; Mobin, M.; Hajibabaei, K.; Ghani, M. Approaches to the Construction of Substituted 4-Amino-1H-Pyrrol-2(5H)-Ones. *J. Org. Chem.* **2012**, *77*, 5808−5812.

(16) Yavari, I.; Mokhtarporyani-sanandaj, A.; Moradi, L.; Mirzaei, A. Reaction of Benzoyl Chlorides with Huisgen ' s Zwitterion : Synthesis of Functionalized 2, 5-Dihydro-1 H -Pyrroles and Tetrasubstituted Furans. *Tetrahedron* **2008**, *64* (22), 5221−5225.

(17) Demir, A. S.; Emrullahoglu, M.; Ardahan, G. New Approaches to Polysubstituted Pyrroles and Pyrrolinones from α-Cyanomethyl-β-Ketoesters. *Tetrahedron* **2007**, *63* (2), 461−468.

(18) Rubottom, G. M.; Pichardo, J. L. Synthesis of N-t-Butyl Benzamides. *Synth. Commun.* **1973**, *3* (3), 185−188.

(19) Flores, A. F. C.; Pizzuti, L.; Piovesan, L. A.; Flores, D. C.; Malavolta, J. L.; Pereira, C. M. P. Efficient synthesis of new 1-alkyl(aryl)-5-(3,3,3-trihalo-2-oxopropylidene)-1H-pyrrol-2(5H)-ones. *Tetrahedron Lett.* **2010**, *51* (37), 4908−4910.

(20) Alves, J. C. F. Preliminary Studies towards the Preparation of Reactive 3-Pyrrolin-2-Ones in Conjugate Addition Reactions for the Syntheses of Potentially Bioactive 2-pyrrolidinones and pyrrolidines. *J. Braz. Chem. Soc.* **2007**, *18* (4), 855−859.

(21) Niknam, K.; Mojikhalifeh, S. Synthesis of New 1,5-Diaryl-3-(Arylamino)-1H-Pyrrol-2(5H)-Ones under Catalyst-Free and Solvent-Free Conditions. *Mol. Diversity* **2014**, *18* (1), 111−117.

(22) Sun, J.; Wu, Q.; Xia, E.-Y.; Yan, C.-G. Molecular Diversity of Three-Component Reactions of Aromatic Aldehydes, Arylamines, and Acetylenedicarboxylates. *Eur. J. Org. Chem.* **2011**, *2011* (16), 2981−2986.

(23) Ye, Y.; Fang, F.; Li, Y. Synthesis and Anti-Biofilm Activities of Dihydro-Pyrrol-2-One Derivatives on Pseudomonas Aeruginosa. *Bioorg. Med. Chem. Lett.* **2015**, *25* (3), 597−601.

(24) Clima, L.; Craciun, B. F.; Angeli, A.; Petreni, A.; Bonardi, A.; Nocentini, A.; Carta, F.; Gratteri, P.; Pinteala, M.; Supuran, C. T. Synthesis, Computational Studies and Assessment of in Vitro Activity of Squalene Derivatives as Carbonic Anhydrase Inhibitors. *ChemMedChem* **2020**, *15* (21), 2052−2057.

(25) Luchinat, E.; Barbieri, L.; Cremonini, M.; Nocentini, A.; Supuran, C. T.; Banci, L. Intracellular Binding/Unbinding Kinetics of Approved Drugs to Carbonic Anhydrase II Observed by in-Cell NMR. *ACS Chem. Biol.* **2020**, *15* (10), 2792−2800.

(26) Angeli, A.; Ferraroni, M.; Da'dara, A. A.; Selleri, S.; Pinteala, M.; Carta, F.; Skelly, P. J.; Supuran, C. T. Structural Insights into Schistosoma Mansoni Carbonic Anhydrase (SmCA) Inhibition by Selenoureido-Substituted Benzenesulfonamides. *J. Med. Chem.* **2021**, *64* (14), 10418−10428.

(27) Mishra, C. B.; Kumari, S.; Angeli, A.; Bua, S.; Tiwari, M.; Supuran, C. T. Discovery of Benzenesulfonamide Derivatives as Carbonic Anhydrase Inhibitors with Effective Anticonvulsant Action: Design, Synthesis, and Pharmacological Evaluation. *J. Med. Chem.* **2018**, *61* (7), 3151−3165.

(28) Angeli, A.; Kartsev, V.; Petrou, A.; Pinteala, M.; Brovarets, V.; Slyvchuk, S.; Pilyo, S.; Geronikaki, A.; Supuran, C. T. Chromene-

https://doi.org/10.1021/acs.jmedchem.3c02190
J. Med. Chem. 2024, 67, 3018−3038

Containing Aromatic Sulfonamides with Carbonic Anhydrase Inhibitory Properties. *Int. J. Mol. Sci.* **2021**, *22* (10), 5082−5097.
(29) McDonald, P. C.; Chafe, S. C.; Brown, W. S.; Saberi, S.; Swayampakula, M.; Venkateswaran, G.; Nemirovsky, O.; Gillespie, J. A.; Karasinska, J. M.; Kalloger, S. E.; Supuran, C. T.; Schaeffer, D. F.; Bashashati, A.; Shah, S. P.; Topham, J. T.; Yapp, D. T.; Li, J.; Renouf, D. J.; Stanger, B. Z.; Dedhar, S. Regulation of PH by Carbonic Anhydrase 9 Mediates Survival of Pancreatic Cancer Cells With Activated KRAS in Response to Hypoxia. *Gastroenterology* **2019**, *157* (3), 823−837.
(30) Al Matarneh, C. M.; Apostu, M. O.; Mangalagiu, I. I.; Danac, R. Reactions of Ethyl Cyanoformate with Cycloimmonium Salts: A Direct Pathway to Fused or Substituted Azaheterocycles. *Tetrahedron* **2016**, *72* (29), 4230−4238.
(31) Al Matarneh, C. M.; Ciobanu, C. I.; Apostu, M. O.; Mangalagiu, I. I.; Danac, R. Cycloaddition versus Amidation in Reactions of 2-Amino-2-Oxoethyl-Phenanthrolinium Ylides to Activated Alkynes and Alkenes. *C. R. Chim.* **2018**, *21* (1), 1−8.
(32) Al-Matarneh, C.; Rosca, I.; Shova, S.; Danac, R. Synthesis and Properties of New Fused Pyrrolo-1,10-Phenanthroline Type Derivatives. *J. Serb. Chem. Soc.* **2021**, *86* (10), 901−915.
(33) Al Matarneh, C. M.; Sardaru, M. C.; Apostu, M. O.; Rosca, I.; Ciobanu, C. I.; Mangalagiu, I. I.; Danac, R. Synthesis and Antibacterial Evaluation of New Pyrrolo[3′,4′:3,4]Pyrrolo[1,2-a]-Quinoline and Pyrrolo[3′,4′:3,4]Pyrrolo[2,1-a]Isoquinoline Derivatives. *Stud. Univ. Babes-Bolyai, Chem.* **2019**, *64* (3), 67−80.
(34) Al Matarneh, C. M.; Mangalagiu, I. I.; Shova, S.; Danac, R. Synthesis, Structure, Antimycobacterial and Anticancer Evaluation of New Pyrrolo-Phenanthroline Derivatives. *J. Enzyme Inhib. Med. Chem.* **2016**, *31* (3), 470−480.
(35) Matarneh, C. A.; Ciobanu, C. I.; Mangalagiu, V.; Zbancioc, G.; Danac, R. Microwave Assisted Synthesis of Six Member Ring Azaheterocycles and Their Antimycobacterial and Anticancer Evaluation. *Rev. Chim.* **2020**, *71* (3), 287−293.
(36) Al Matarneh, C. M.; Amarandi, R. M.; Craciun, A. M.; Mangalagiu, I. I.; Zbancioc, G.; Danac, R. Design, Synthesis, Molecular Modelling and Anticancer Activities of New Fused Phenanthrolines. *Molecules* **2020**, *25* (3), 527−543.
(37) Sardaru, M. C.; Craciun, A. M.; Al Matarneh, C. M.; Sandu, I. A.; Amarandi, R. M.; Popovici, L.; Ciobanu, C. I.; Peptanariu, D.; Pinteala, M.; Mangalagiu, I. I.; Danac, R. Cytotoxic Substituted Indolizines as New Colchicine Site Tubulin Polymerisation Inhibitors. *J. Enzyme Inhib. Med. Chem.* **2020**, *35* (1), 1581−1595.
(38) Al-Matarneh, M. C.; Amărandi, R.-M.; Mangalagiu, I. I.; Danac, R. Synthesis and Biological Screening of New Cyano-Substituted Pyrrole Fused (Iso)Quinoline Derivatives. *Molecules* **2021**, *26* (7), 2066−2085.
(39) Danac, R.; Al Matarneh, C. M.; Shova, S.; Daniloaia, T.; Balan, M.; Mangalagiu, I. I. New Indolizines with Phenanthroline Skeleton: Synthesis, Structure, Antimycobacterial and Anticancer Evaluation. *Bioorg. Med. Chem.* **2015**, *23* (10), 2318−2327.
(40) Angeli, A.; Kartsev, V.; Petrou, A.; Lichitsky, B.; Komogortsev, A.; Pinteala, M.; Geronikaki, A.; Supuran, C. T. Pyrazolo[4,3-c]Pyridine Sulfonamides as Carbonic Anhydrase Inhibitors: Synthesis, Biological and In Silico Studies. *Pharmaceuticals* **2022**, *15* (3), 316−339.
(41) Angeli, A.; Kartsev, V.; Petrou, A.; Pinteala, M.; Vydzhak, R. M.; Panchishin, S. Y.; Brovarets, V.; De Luca, V.; Capasso, C.; Geronikaki, A.; Supuran, C. T. New Sulfanilamide Derivatives Incorporating Heterocyclic Carboxamide Moieties as Carbonic Anhydrase Inhibitors. *Pharmaceuticals* **2021**, *14* (8), 828.
(42) Angeli, A.; Kartsev, V.; Petrou, A.; Pinteala, M.; Brovarets, V.; Vydzhak, R.; Panchishin, S.; Geronikaki, A.; Supuran, C. T. Carbonic Anhydrase Inhibition with Sulfonamides Incorporating Pyrazole- and Pyridazinecarboxamide Moieties Provides Examples of Isoform-Selective Inhibitors. *Molecules* **2021**, *26* (22), 7023−7040.
(43) Petreni, A.; Iacobescu, A.; Simionescu, N.; Petrovici, A.-R.; Angeli, A.; Fifere, A.; Pinteala, M.; Supuran, C. T. Carbonic Anhydrase Inhibitors Bearing Organotelluride Moieties as Novel Agents for Antitumor Therapy. *Eur. J. Med. Chem.* **2022**, *244*, No. 114811.
(44) Ferraroni, M.; Angeli, A.; Pinteala, M.; Supuran, C. T. Sulfonamide Diuretic Azosemide as an Efficient Carbonic Anhydrase Inhibitor. *J. Mol. Struct.* **2022**, *1268*, No. 133672.
(45) Angeli, A.; Pinteala, M.; Maier, S. S.; Toti, A.; Mannelli, L. D. C.; Ghelardini, C.; Selleri, S.; Carta, F.; Supuran, C. T. Tellurides Bearing Benzensulfonamide as Carbonic Anhydrase Inhibitors with Potent Antitumor Activity. *Bioorg. Med. Chem. Lett.* **2021**, *45*, No. 128147.
(46) Weber, L.; Illgen, K.; Almstetter, M. Discovery of New Multi Component Reactions with Combinatorial Methods. *Synlett* **1999**, *1999* (3), 366−374.
(47) Parr, R. G.; Yang, W. *Density Functional Theory of Atoms and Molecules*; Oxford University Press: New York, 1995.
(48) Parr, R. G.; Yang, W. Density Functional Approach to the Frontier-Electron Theory of Chemical Reactivity. *J. Am. Chem. Soc.* **1984**, *106* (14), 4049−4050.
(49) Khalifah, R. G. The Carbon Dioxide Hydration Activity of Carbonic Anhydrase. *J. Biol. Chem.* **1971**, *246* (8), 2561−2573.
(50) Angeli, A.; Micheli, L.; Turnaturi, R.; Pasquinucci, L.; Parenti, C.; Alterio, V.; Di Fiore, A.; De Simone, G.; Monti, S. M.; Carta, F.; Di Cesare Mannelli, L.; Ghelardini, C.; Supuran, C. T. Discovery of a Novel Series of Potent Carbonic Anhydrase Inhibitors with Selective Affinity for μ Opioid Receptor for Safer and Long-Lasting Analgesia. *Eur. J. Med. Chem.* **2023**, *260*, No. 115783.
(51) Srivastava, D. K.; Jude, K. M.; Banerjee, A. L.; Haldar, M.; Manokaran, S.; Kooren, J.; Mallik, S.; Christianson, D. W. Structural Analysis of Charge Discrimination in the Binding of Inhibitors to Human Carbonic Anhydrases I and II. *J. Am. Chem. Soc.* **2007**, *129* (17), 5528−5537.
(52) Behnke, C. A.; Le Trong, I.; Godden, J. W.; Merritt, E. A.; Teller, D. C.; Bajorath, J.; Stenkamp, R. E. Atomic Resolution Studies of Carbonic Anhydrase II. *Acta Crystallogr., Sect. D: Biol. Crystallogr.* **2010**, *66* (5), 616−627.
(53) Leitans, J.; Kazaks, A.; Balode, A.; Ivanova, J.; Zalubovskis, R.; Supuran, C. T.; Tars, K. Efficient Expression and Crystallization System of Cancer-Associated Carbonic Anhydrase Isoform IX. *J. Med. Chem.* **2015**, *58* (22), 9004−9009.
(54) Whittington, D. A.; Waheed, A.; Ulmasov, B.; Shah, G. N.; Grubb, J. H.; Sly, W. S.; Christianson, D. W. Crystal Structure of the Dimeric Extracellular Domain of Human Carbonic Anhydrase XII, a Bitopic Membrane Protein Overexpressed in Certain Cancer Tumor Cells. *Proc. Natl. Acad. Sci. U.S.A.* **2001**, *98* (17), 9545−9550.
(55) D'Ascenzio, M.; Secci, D.; Carradori, S.; Zara, S.; Guglielmi, P.; Cirilli, R.; Pierini, M.; Poli, G.; Tuccinardi, T.; Angeli, A.; Supuran, C. T. 1,3-Dipolar Cycloaddition, HPLC Enantioseparation, and Docking Studies of Saccharin/Isoxazole and Saccharin/Isoxazoline Derivatives as Selective Carbonic Anhydrase IX and XII Inhibitors. *J. Med. Chem.* **2020**, *63* (5), 2470−2488.
(56) Pontecorvi, V.; Mori, M.; Picarazzi, F.; Zara, S.; Carradori, S.; Cataldi, A.; Angeli, A.; Berrino, E.; Chimenti, P.; Ciogli, A.; Secci, D.; Guglielmi, P.; Supuran, C. T. Novel Insights on Human Carbonic Anhydrase Inhibitors Based on Coumalic Acid: Design, Synthesis, Molecular Modeling Investigation, and Biological Studies. *Int. J. Mol. Sci.* **2022**, *23* (14), 7950.
(57) Frisch, M. J.; Trucks, G. W.; Schlegel, H. B.; Scuseria, G. E.; Robb, M. A.; Cheeseman, J. R.; Scalmani, G.; Barone, V.; Petersson, G. A.; Nakatsuji, H.; Li, X.; Caricato, M.; Marenich, A. V.; Bloino, J.; Janesko, B. G.; Gomperts, R.; Mennucci, B.; Hratchian, H. P.; Ortiz, J. V.; Klene, M.; Adamo, C.; Cammi, R.; Ochterski, J. W.; Martin, R. L.; Morokuma, K.; Farkas, O.; Foresman, J. B.; Fox, D. J. *Gaussian 16*, Revision C.01; Gaussian, Inc.: Wallingford CT, 2016.
(58) Zhang, Z.; Vasiliu, T.; Li, F.; Laaksonen, A.; Zhang, X.; Mocci, F.; Ji, X. Novel Artificial Ionic Cofactors for Efficient Electro-Enzymatic Conversion of CO2 to Formic Acid. *J. CO2 Util.* **2022**, *60*, No. 101978.

https://doi.org/10.1021/acs.jmedchem.3c02190
J. Med. Chem. 2024, 67, 3018−3038

(59) Melis, N.; Mocci, F.; Vacca, A.; Pilia, L. Sulphur vs NH Group: Effects on the CO2 Electroreduction Capability of Phenylenediamine-Cp Cobalt Complexes. *Molecules* **2023**, *28* (5), 2364.
(60) Melis, N.; Mocci, F.; Vacca, A.; Pilia, L. Novel Homogeneous Selective Electrocatalysts for CO2reduction: An Electrochemical and Computational Study of Cyclopentadienyl-Phenylendiamino-Cobalt Complexes. *Sustainable Energy Fuels* **2020**, *4* (11), 5609−5617.
(61) Lu, T.; Chen, F. Atomic Dipole Moment Corrected Hirshfeld Population Method. *J. Theory Comput. Chem.* **2012**, *11* (1), 163−183.
(62) Lu, T.; Chen, F. Multiwfn: A Multifunctional Wavefunction Analyzer. *J. Comput. Chem.* **2012**, *33* (5), 580−592.
(63) Humphrey, W.; Dalke, A.; Schulten, K. VMD:Visual Molecular Dynamics. *J. Mol. Graphics* **1996**, *14*, 33−38.
(64) Supuran, C. T. Carbonic Anhydrase Inhibitors and Activators for Novel Therapeutic Applications. *Future Med. Chem.* **2011**, *3* (9), 1165−1180.
(65) Angeli, A.; Micheli, L.; Carta, F.; Ferraroni, M.; Pirali, T.; Fernandez Carvajal, A.; Ferrer Montiel, A.; Di Cesare Mannelli, L.; Ghelardini, C.; Supuran, C. T. First-in-Class Dual Hybrid Carbonic Anhydrase Inhibitors and Transient Receptor Potential Vanilloid 1 Agonists Revert Oxaliplatin-Induced Neuropathy. *J. Med. Chem.* **2023**, *66* (2), 1616−1633.
(66) Angeli, A.; Ferraroni, M.; Supuran, C. T. Famotidine, an Antiulcer Agent, Strongly Inhibits Helicobacter Pylori and Human Carbonic Anhydrases. *ACS Med. Chem. Lett.* **2018**, *9* (10), 1035−1038.
(67) Angeli, A.; Trallori, E.; Carta, F.; Di Cesare Mannelli, L.; Ghelardini, C.; Supuran, C. T. Heterocoumarins Are Selective Carbonic Anhydrase IX and XII Inhibitors with Cytotoxic Effects against Cancer Cells Lines. *ACS Med. Chem. Lett.* **2018**, *9* (9), 947−951.
(68) Burley, S. K.; Bhikadiya, C.; Bi, C.; Bittrich, S.; Chen, L.; Crichlow, G. V.; Christie, C. H.; Dalenberg, K.; Di Costanzo, L.; Duarte, J. M.; Dutta, S.; Feng, Z.; Ganesan, S.; Goodsell, D. S.; Ghosh, S.; Green, R. K.; Guranovic, V.; Guzenko, D.; Hudson, B. P.; Lawson, C. L.; Liang, Y.; Lowe, R.; Namkoong, H.; Peisach, E.; Persikova, I.; Randle, C.; Rose, A.; Rose, Y.; Sali, A.; Segura, J.; Sekharan, M.; Shao, C.; Tao, Y. P.; Voigt, M.; Westbrook, J. D.; Young, J. Y.; Zardecki, C.; Zhuravleva, M. RCSB Protein Data Bank: Powerful New Tools for Exploring 3D Structures of Biological Macromolecules for Basic and Applied Research and Education in Fundamental Biology, Biomedicine, Biotechnology, Bioengineering and Energy Sciences. *Nucleic Acids Res.* **2021**, *49* (1), D437−D451.
(69) Monvall, E. Statsbudgeten: De Stora Reformerna Gäller Arbetslivet. *Tidskr. Sver. Sjukskot.* **1976**, *43* (2), 54−58.
(70) Lu, C.; Wu, C.; Ghoreishi, D.; Chen, W.; Wang, L.; Damm, W.; Ross, G. A.; Dahlgren, M. K.; Russell, E.; Von Bargen, C. D.; Abel, R.; Friesner, R. A.; Harder, E. D. OPLS4: Improving Force Field Accuracy on Challenging Regimes of Chemical Space. *J. Chem. Theory Comput.* **2021**, *17* (7), 4291−4300.
(71) Ragab, M. A.; Eldehna, W. M.; Nocentini, A.; Bonardi, A.; Okda, H. E.; Elgendy, B.; Ibrahim, T. S.; Abd-Alhaseeb, M. M.; Gratteri, P.; Supuran, C. T.; Al-Karmalawy, A. A.; Elagawany, M. 4-(5-Amino-Pyrazol-1-Yl)Benzenesulfonamide Derivatives as Novel Multi-Target Anti-Inflammatory Agents Endowed with Inhibitory Activity against COX-2, 5-LOX and Carbonic Anhydrase: Design, Synthesis, and Biological Assessments. *Eur. J. Med. Chem.* **2023**, *250*, No. 115180.
(72) Sbravati, D.; Bonardi, A.; Bua, S.; Angeli, A.; Ferraroni, M.; Nocentini, A.; Casnati, A.; Gratteri, P.; Sansone, F.; Supuran, C. T. Calixarenes Incorporating Sulfonamide Moieties: Versatile Ligands for Carbonic Anhydrases Inhibition. *Chem. − Eur. J.* **2022**, *28* (6), No. e202103527.
(73) Schrödinger. Schrödinger Suite Release 2022−2: New York 2022. https://www.schrodinger.com/products/glide.
(74) Schrödinger. Schrödinger Suite Release 2022−2: New York. https://www.schrodinger.com/products/maestro.
(75) Schrödinger. Schrödinger Suite Release 2022−2: New York 2022. https://www.schrodinger.com/products/macromodel.
(76) Schrödinger. Schrödinger Suite Release 2022−2: New York 2022.
(77) Schrödinger. Schrödinger Suite Release 2022−2: New York 2022. https://www.schrodinger.com/products/desmond.
(78) Pettersen, E. F.; Goddard, T. D.; Huang, C. C.; Couch, G. S.; Greenblatt, D. M.; Meng, E. C.; Ferrin, T. E. UCSF Chimera - A Visualization System for Exploratory Research and Analysis. *J. Comput. Chem.* **2004**, *25* (13), 1605−1612.
(79) Leslie, A. G. W.; Powell, H. R. Procesing Diffraction Data with Mosflm. In *Evolving Methods for Macromolecular Crystallography*; Read, R. J.; Sussman, J.L., Eds.; NATO Science Series II: Mathematics, Physics and Chemistry; Springer: Dordrecht, 2007.
(80) Murshudov, G. N.; Vagin, A. A.; Dodson, E. J. Refinement of Macromolecular Structures by the Maximum-Likelihood Method. *Acta Crystallogr., Sect. D: Biol. Crystallogr.* **1997**, *53* (3), 240−255.
(81) Emsley, P.; Lohkamp, B.; Scott, W. G.; Cowtan, K. Features and Development of Coot. *Acta Crystallogr., Sect. D: Biol. Crystallogr.* **2010**, *66* (4), 486−501.
(82) Lovell, S. C.; Davis, I. W.; Arendall, W. B.; de Bakker, P. I. W.; Word, J. M.; Prisant, M. G.; Richardson, J. S.; Richardson, D. C. Structure Validation by Cα Geometry: ϕ,ψ and Cβ Deviation. *Proteins: Struct., Funct., Bioinf.* **2003**, *50* (3), 437−450.

https://doi.org/10.1021/acs.jmedchem.3c02190
J. Med. Chem. 2024, 67, 3018−3038